UNIVERSITY OF CALIFORNIA,

IRVINE

**Analysis of Near-Infrared Image to Diagnose Maxillary Sinusitis**

THESIS

submitted in partial satisfaction of the requirements for the degree of

MASTER OF SCIENCE

in Biomedical Engineering

by

Maryamsadat Amini

Thesis Committee:

Professor Bruce Tromberg, Chair
Associate Professor Gultekin Gulsen
Assistant Researcher Albert Cerussi

2014

# TABLE OF CONTENTS

# LIST OF FIGURES

# LIST OF TABLES

Table Page

# ACKNOWLEDGEMENTS

First and foremost I offer my sincerest gratitude to my supervisor, Dr. Albert Cerussi, who has supported me throughout my master thesis with his patience and knowledge. I am grateful to him for everything. Special thanks go to Dr. Bruce Tromberg who has supported me as my advisor during this time.

I am thankful to Dr. Gultekin Gulsin to be part of my thesis committee. Also, I would like to thank all the undergraduate students and staff for providing near-infrared images to do this research.

Last but not the least, I would like to thank my family: my parents Mostafa Amini and Hamideh Hosseini, for giving me life and supporting me financially and spiritually throughout my life.

# ABSTRACT

ANALYSIS OF NEAR-INFRARED IMAGE TO DIAGNOSE MAXILLARY SINUSITIS

By

Maryamsadat Amini

Master of Science in Biomedical Engineering

University of California, Irvine, 2014

Professor Bruce Tromberg, Chair

**Introduction:** Sinusitis is one of the most common chronic illnesses. Computed tomography is the most common imaging method in sinusitis detection. **Objectives:** The main purpose of this study is to determine the diagnostic usage of NIR imaging in maxillary sinusitis. It is also determined which feature set produces the most efficient classification results. In addition, it is investigated whether the color normalization of the NIR images affects on the results. **Results:** Histogram mean, texture inertia, and texture entropy are the most efficient features in data discrimination. The best sensitivity in maxillary sinusitis detection is 76% produced by using asymmetry indicator values of histogram mean feature extracted from the original images. In addition, the discrimination functionality of the selected feature set is degraded by color normalization. **Methods:** After the NIR images are prepared, their regions of interest (ROI) are selected manually. Then several features are extracted from the images. The values are used to measure a feature-based asymmetry indicator according to the left and right

maxillary sinuses in each image. Also, the images of test class (test set) can be classified by having the range of the asymmetry indicator for control and sever images (train set). The classification correctness metrics are calculated to evaluate the diagnostic role of NIR images in sinusitis disease. **Conclusion:** It is possible to detect sinusitis using NIR imaging with the sensitivity of 76%. The most effective feature for maxillary sinusitis detection is histogram mean feature. Color normalization is not recommended to be applied on the images.

# CHAPTER 1

# INTRODUCTION

Sinusitis is an inflammation of the tissue that lines the paranasal sinuses. The paranasal sinuses are four pair of cavities that are normally filled by the air and named according to the facial bone in which they are located; maxillary sinuses, frontal sinuses, ethmoidal sinuses, and sphenoidal sinuses. Figure 1.1 illustrates healthy sinus cavities versus inflamed sinuses in a sinusitis condition.

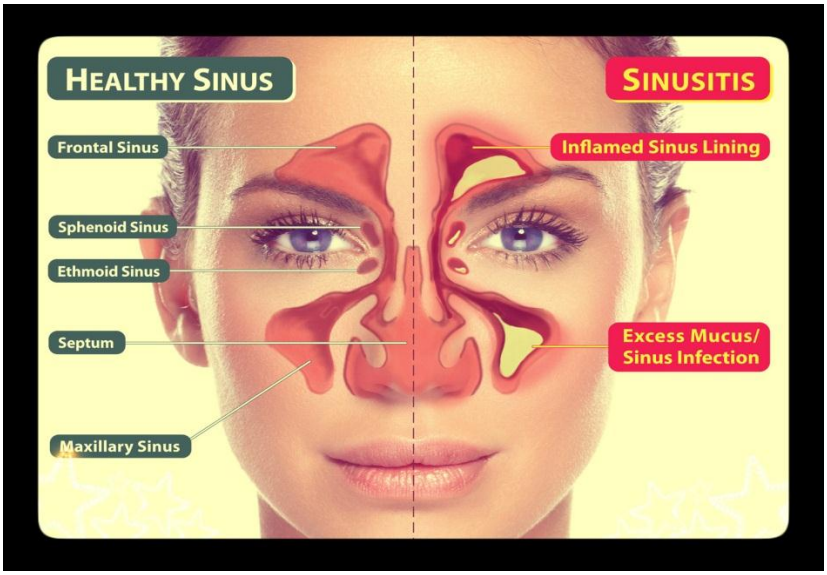


**Figure 1.1: Healthy sinus and sinusitis**

The paranasal sinuses are connected to the nasal cavity through small openings called ostia. Any blockage in these openings disrupts the drainage functionality of sinuses which leads to fluid-filled sinuses and thus infection [1]. Sinusitis is one of the most common chronic illnesses [2, 3], which affects approximately 12% of individuals below the age of 45 years in the United States [4], and results in a significant antibiotic usage as one of the common treatments [5].

Currently, the diagnosis methods applied by the primary care physicians are the patient's symptoms and disease history conveyed by the patient. Moreover, X-rays and computer tomography (CT) imagining methods are implemented for challenging cases to increase the diagnosis accuracy [2, 3]. However, sinusitis diagnosis is still remained controversial for primary care physicians. Diverse diseases with very similar symptoms to sinusitis such as allergic rhinitis and migraine, and inability of the patients (in case of children) to explain their problem accurately are origins of the sinusitis diagnosis debate. In addition, high radiation exposure and cost of the mentioned imaging methods are the concerns patients and physicians have, especially in the pediatric health care.

Therefore, an investigation is dedicated to look for an alternative diagnostic imaging method to detect sinusitis. As the recent significant advancements of the optics has created a silver lining in the field of medical imaging, a novel near-infrared (NIR) imaging system has been introduced as a potential diagnostic imaging method for maxillary sinusitis [2, 3].

In this research study, image processing and data analysis methods are applied to determine if the extracted features from the NIR images can be utilized for maxillary sinusitis detection. The investigation includes four steps:

- Data acquisition and image preprocessing
- Image segmentation
- Feature extraction
- Data analysis and classification

The first step gives information about how the NIR images are maintained and prepared for the next steps with major computational processes. The second step provides only the region of interest (ROI) of the NIR images by image segmentation methods to avoid storage and analysis

of unnecessary information. The ROI is the both left and right maxillary sinuses from each image. In the third step, several features such as histogram and texture features are extracted from the images. In the last step, the extracted information is used to measure a feature-based asymmetry indicator according to the left and right maxillary sinuses in each image. Also, the images of test class (test set) can be classified by having the range of the asymmetry indicator for control and sever images (train set). The classification correctness metrics (or the success rates) such as sensitivity and specificity are calculated to evaluate the diagnostic role of NIR images in sinusitis disease.

## 1.1 Objectives of the Thesis

The main purpose of the research study is to determine the diagnostic usage of NIR imaging in sinusitis. The objectives of the research can be categorized as follows:

- Determine the most efficient feature set to be applied in the classification of the test set
- Identify the usage of NIR images for maxillary sinusitis detection by using original images
- Investigate the image normalization affect on the extracted features and thus classification results

## 1.2 The Thesis Structure

*Chapter 2* provides a literature review of the previous related research studies, overall explanation of conventional imaging methods and specifically the imaging system applied in the research.

*Chapter 3* presents experimental materials and tools used in this study, such as NIR images, their corresponding masks, software and programs.

*Chapter 4* explains all the implemented methods and algorithms, feature extraction, and data analysis besides classification.

*Chapter 5* encompasses the total experimental results and a comprehensive discussion.

*Chapter 6* provides a comprehensive summery with a conclusion.

*Chapter 7* presents the future work which will further develop the research study.

# CHAPTER 2

# LITERATURE REVIEW

## 2.1 Current Imaging Methods of Sinusitis Detection

Diagnostic imaging methods such as computed tomography (CT scan), X-rays, and magnetic resonance imaging (MRI) are the common methods in Sinusitis detection. The following is a brief review of these diagnostic imaging techniques, respectively [2, 3].

### 2.1.1 Computed Tomography (CT)

Currently, computed tomography (CT) scanning is the most reliable imaging method to view the paranasal sinuses. Although, no statistical relationship is found between symptom severity of most patients and CT findings of abnormalities, there is a common clinical belief that CT scan findings may represent the severity of the chronic sinusitis [6]. This imaging method reveals inflamed and infected areas even in deep hidden sinus chambers which are missed by x-rays. However, its relatively high dose of radiation and cost limit the usage of this method. Only chronic and acute sinusitis cases with severe infection and high chance of complications are recommended to use CT scans for more accurate diagnosis [7, 8].

### 2.1.2 X-rays

X-rays imaging system were used commonly before the advent of CT scans. They are not as detailed as CT scans; however multiple x-rays from several directions increase the diagnosing accuracy. For example, Frontal and sphenoid sinusitis can be diagnosed by more than one x-ray. But ethmoid sinusitis is not detected by x-rays at all, which can spread the infection to the maxillary or frontal sinuses [7, 9]. In overall, x-rays have much lower degree of sensitivity than

CT scans which declines their capability as screening tests in sinusitis diagnosis. Therefore, they are not recommended to be used routinely for suspected acute sinusitis [10].

### 2.1.3 Magnetic Resonance Imaging (MRI)

Unlike x-rays and CT scans using radiation, MRI uses powerful magnetic and radio frequency fields to reveal a detailed image of the sinuses [11]. This imaging method can help to diagnose fungal sinusitis, malignant tumors, and other inflammatory diseases. However, since MRI is not able to define the paranasal anatomy as effective as CT scans, physicians do not recommend it as a diagnostic method for suspected sinusitis, typically [7]. Although, MRI does not use radiation and its contrasting agent is less likely to have an allergic reaction, but its high cost is one of the most important concerns. Regarding all the difficulties of the conventional imaging methods, there is a motivation to find an alternative diagnostic method which is radiationless and cost-efficient.

## 2.2 Near-infrared Imaging (NIR Imaging)

Near-infrared (NIR) Imaging is an imaging method based on the detection of transilluminated NIR radiation by the corresponding detector. Transillumination technique is used to illuminate a sample (an organ or part of the body) by passing strong light through it. One of its main applications is the detection of abnormalities and diseases in a part of body. NIR refers to electromagnetic radiation with wavelength range from about 750nm to 1100nm, which has a low absorption rate by water and hemoglobin (the main components of the biological tissues) [2, 3]. This fact increases the penetration depth of the NIR through the tissue which results in illumination of deeper tissues and high depth resolution of the imaging system.

Similar to the most of the imaging systems, NIR imaging system includes two principal parts: a source and a detector. A source is a device to produce the NIR light, and a detector is a camera sensitive to NIR wavelength to capture and create images.

The most prevalent sources of NIR radiation are common incandescent or quartz halogen light bulbs. Also, light-emitting diodes (LEDs) are used as the NIR light sources. They provide longer lifetime, stable spectrum, and less power supplies [12]. The type of the detector is selected based on the wavelengths range to be measured. For example, for the shorter end of the NIR range, silicon-based charge-coupled devices (CCDs) are useful and efficient. However, they are not sensitive enough for wavelengths range over 1000 nm.

### 2.2.1 Theory

The theory of NIR imaging system leans on the transillumination fact which is illumination of a matter through which the light is transmitted. The transmitted light from the matter does not have the same intensity as the incident light which is sent out from the source and enters the matter. The light intensity is attenuated by absorption and scattering through its trip inside of a material. Attenuation coefficient is a measurement to characterize different materials based on how easy they can be penetrated by a specific light or radiation. Larger attenuation coefficient results in faster attenuation or weakening of the light as it passes through the material. However, a material with a smaller attenuation coefficient is relatively transparent to the light. The quantity of the attenuation coefficient is described by the Beer-Lambert law, in which the intensity of transmitted light $\boldsymbol{I}$ through a material with the thickness of $\boldsymbol{x}$ and attenuation coefficient of $\boldsymbol{\alpha}$ is related to the incident intensity $\boldsymbol{I_0}$, exponentially [13]:

$$I = I_0 e^{-\alpha x}$$

As sinusitis changes the structure and material of the sinuses, the normal attenuation coefficient of that area is affected and increased. Therefore, the transmitted NIR intensity captured by the detector (camera) of the imaging system is reduced. The purpose of this research study is to determine whether this fact can be detected in the captured images and use it as a potential diagnosis factor.

## 2.3 History

In 1989, one of the first investigations was devoted to evaluate the reliability of transillumination method for diagnosis purpose of maxillary sinusitis in children. In this research, a diaphanoscope was used as the light source and located inside of the subject's mouth. There was no detector or camera, but an investigator evaluated the degree of illumination of the soft tissue anterior to the maxillary sinuses. The labels 'good' or 'poor' were used to classify the illumination qualification results. The estimated results of the illumination were compared by the drainage findings, which revealed a low sensitivity. Also, no specificity result was reported in this research study due to lack of their control subjects. The low sensitivity and unreliable results lead the transillumination method to be denied as a diagnostic method [14].

Despite the unreliable results obtained by the trasillumination in the twentieth century, this method is still listed as a physical examination in the clinical practical guide and used by medical students and health care team [15].

# CHAPTER 3

# EXPERIMENTAL MATERIALS AND TOOLS

The materials and tools utilized in this research include a NIR imaging system, NIR images, manually created masks, and three programs. CVIPtools and CVIP-FEPC are the main programs used which are developed at Southern Illinois University at Edwardsville (SIUE). In addition, the Microsoft Excel is applied in data retrieval and data analysis phase of the research.

## 3.1 NIR Imaging System

The NIR Imaging system used in this research relies on the transillumination technique. This imaging system includes two main parts: a light source and a detector. The light source is powered by a Hewlett Packard Power Source and made of different parts. The main part which generates the required NIR light is two parallel series of four LEDs (Roithner Lasertechnik, Vienna, Austria). One of the LEDs series emits light with a wavelength of 810nm (1mW) and the other one produces light with a wavelength of 850nm (1mW). The combination of the LEDs is selected due to their optimal tissue penetration in the previous experiments. The LEDs are isolated by a capsule with the shape of a spoon opposed to a flat base with a handle. As it is shown in Figure 3.1, the LEDs are located on the flat base of the light source and soldered onto power wires. The arch-shaped structure of the light source is used because it fits well with the mouth structure and hard palate. This capsule is made of clear acrylic which allows NIR light transmission with no obstruction, and also is light-weight, non-toxic, durable, and sterilizable for frequent patient usage. The edge between the arch-shaped surface and the flat base is covered by a rubber gasket to isolate the electrical components from the water for the patients' safety. In

addition, the surface of the flat base, underneath of the LEDs, is covered by a copper tape to reflect the scattered light and reduce the light lost [2, 3].

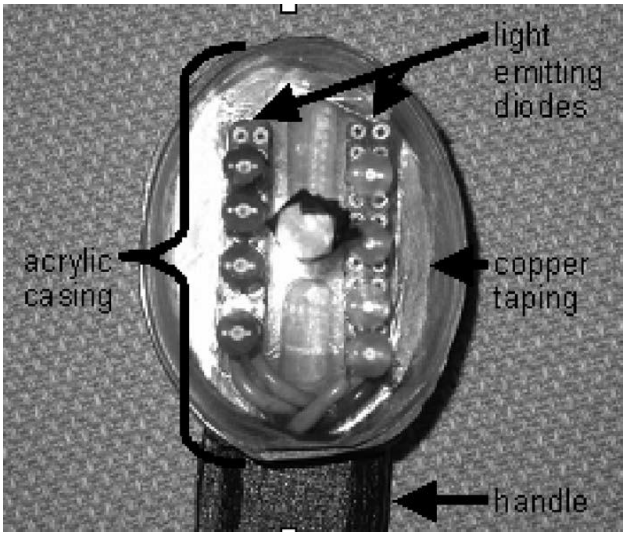


**Figure 3.1: NIR Imaging System**

The detector of this imaging system is a silicon-based CCD video camera with the sensitivity to NIR signal by removing its infrared filter (Marlin P. Jones and Associates, Lake Park, Florida, USA). A five volt power supply is used to power the camera. After the images are recorded by the camera, they are stored into a notebook PC via a RCA-to-USB adapter by using video capturing software (Pinnacle Linx Studio 7.0, Pinnacle Systems Inc., Mountain View, California, USA). The proposed NIR imaging system excluding the PC costs less than 100$ which is much more cost-efficient than the current conventional imaging systems for sinusitis diagnosis [2, 3].

## 3.2 The NIR Images

The NIR images were taken from several patients and volunteers with normal sinuses. The patients are in the age of 15 or older undergoing clinical cares of sinusitis or similar diseases at the Otolaryngology-Head and Neck Surgery Clinic at the University of California at Irvine

Medical Center. All the patients were subject to obtaining CT images [2, 3]. The healthy volunteers are non-symptomatic cases who are adults. Their NIR images will be mainly used to determine the signal variation from measurement to measurement, rather than absolute diagnosis.

Depending on penetration depth of the NIR light through the tissues, different parts of the face are illuminated in the images. Hard and thick tissues or biological materials with high absorption rate block the NIR light passage. These areas are appeared in very dark or black colors in the images. Cheekbones and any infections and fluids inside of the sinus cavities are samples of the dark areas in the NIR images. There are two NIR sample images from a normal case and a patient with a sinus abnormality, which are illustrated respectively in Figure 3.2 and Figure 3.3.

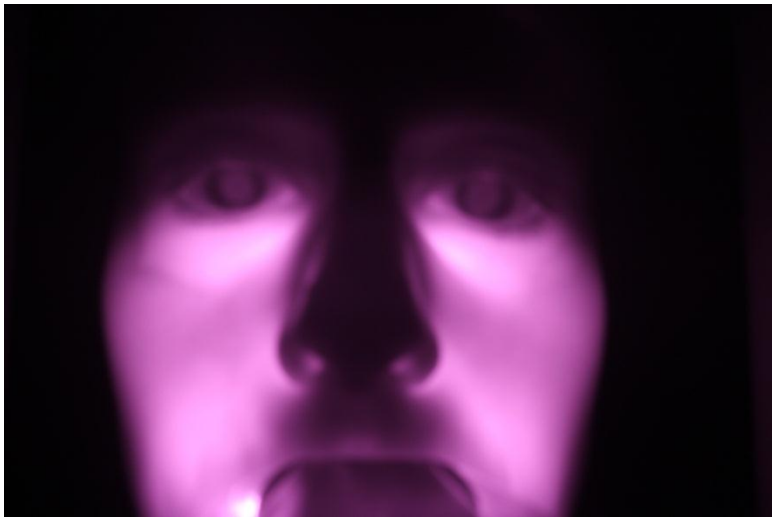

**Figure 3.2: NIR image from a normal case (control case)**

**Figure 3.3: NIR image from a patient with sinus abnormality on the left side (sever case)**

Each of the images includes 4272×2848 pixels with the total size of about 2MB. These images are pretty big and engage high percentage of the CPU usage while being processed. So there is a need of preprocessing step to decrease the image size and time required for image analysis. The detail attributes of the NIR images are shown in Table **3.1**.

**Table 3.1: NIR Image Attributes**

| | |
|---|---|
| **Image size** | 4272×2848 pixels |
| **Image format** | JPG |
| **Color format** | RGB |
| **Data format** | Real |
| **Data type** | Byte (0-255) |

In this research study, a total number of 180 NIR images are processed. The images are taken from 12 Patients (abnormal cases) and 6 healthy volunteers (normal cases). All the images

can be also categorized into three classes of *control*, *sever*, and *test*. The *control* class includes the NIR images captured from normal cases. The NIR images from abnormal cases with obvious visual differences between their left and right sinuses are collected in the *sever* class. The most interesting class is the *test*, which includes NIR images taken from both normal and abnormal cases. However unlike the *sever* class, the images from abnormal cases in the *test* class are very challenging to be diagnosed visually. Also, the normal images gathered in the *test* class are not the same as *control* class images. The number of NIR images in each of the classes is illustrated in Table 3.2.

**Table 3.2: Number of NIR Images in Each Class**

| **The Number of Images** | | | |
|---|---|---|---|
| Control | Sever | Test | |
| | | Normal | Abnormal |
| 65 | 65 | 25 | 25 |

As the purpose of this research study is to diagnose sinusitis by using an asymmetry indicator between left and right maxillary sinuses, the regions are subject to being segmented from the original images and processed separately. The approximate regions corresponding to the both left and right maxillary sinuses are depicted in Figure 3.4. There are more details about the segmented regions in the following section of Border Masks.

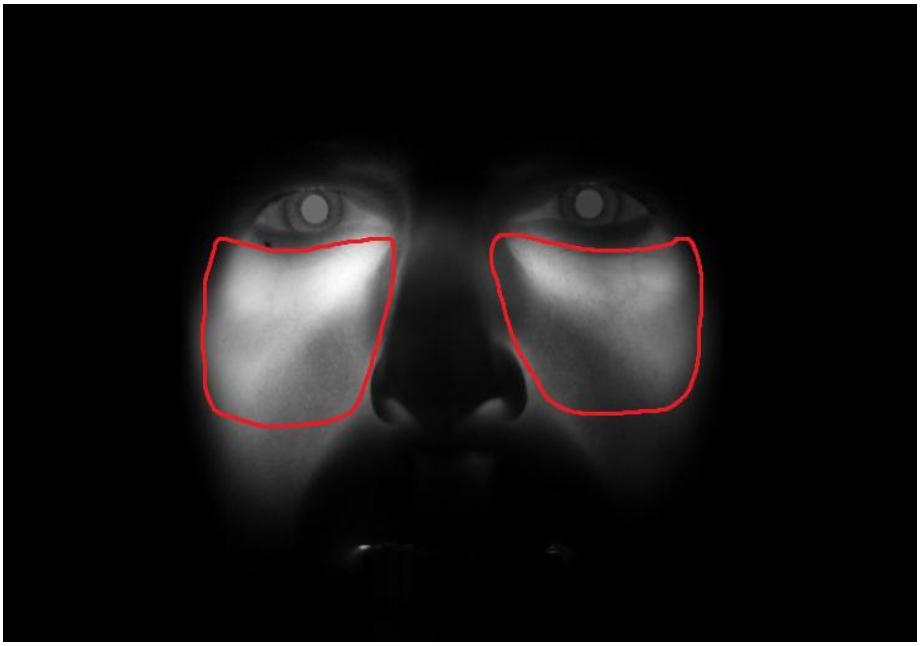

**Figure 3.4: A *Test* Image Sample with Maxillary Sinuses (ROIs) Shown by a Red Border**

## 3.3 Border Masks

Border masks are black and white, binary, images in which pixels with the value of '1' (white) represent the region of interest (ROI). In the image processing, masks are used to restrict the processing to the only ROI (white pixels) of the input images which decreases the required time and memory in the research experiments. In this study, the maxillary sinuses are considered as the regions of interest, which are the largest paranasal sinuses and located under the eyes in the maxillary bones. In this study, the total number of 360 border masks is created manually for both left and right maxillary sinuses. The masks are created by using CVIPtools, with the following steps: *Utilities-> Create-> Border mask*. There is a NIR image with the corresponding masks from its left and right maxillary sinuses illustrated in Figure 3.5.

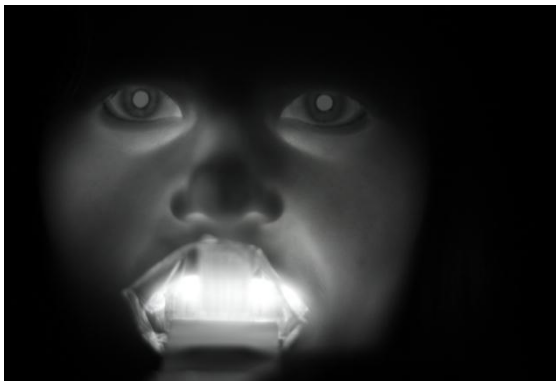

**(a) Original Image**

**(b) Mask Image of Right Maxillary Sinus**

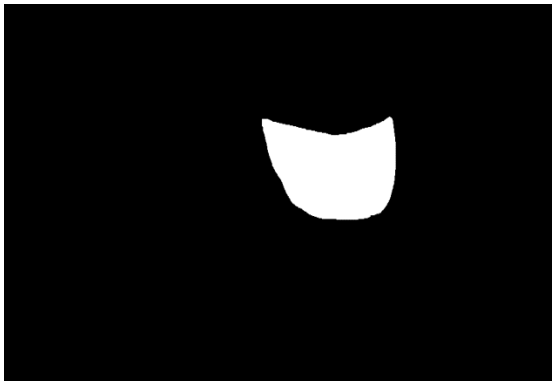

**(c) Mask Image of Left Maxillary Sinus**

**Figure 3.5: (b) and (c) Are Manual Masks Created from Their Corresponding Original Image (a)**

## 3.4 Programs and Algorithms

The programs applied in this study can be categorized in two classes; image processing, and data analysis. There are four image processing programs; CVIPtools, CVIP-ATAT, CVIP-FEPC, and Color Normalization. In order to analyze and visualize the data obtained from image processing techniques, two programs are utilized; Partek Discovery Suite, and Microsoft Excel.

### 3.4.1 CVIPtools v5.3 (Computer Vision and Image Processing Tools)

CVIPtools version 5.3 is the current Windows version, which was developed by the Computer Vision and Image Processing (CVIP) Laboratory in the Department of Electrical and Computer Engineering of Southern Illinois University Edwardsville (SIUE). This software provides the

capability of computer processing of digital images by various imaging functions [16]. CVIPtools allows for the manual processing of one image at a time and produces an instant result.

In this study, the software is applied for manual mask creation and color normalization. The color normalization is implemented by the histogram stretch algorithm. In addition, it is efficient to test an algorithm on one sample image to see the result in a short time.

### 3.4.2 CVIP-FEPC (CVIP Feature Extraction and Pattern Classification)

CVIP-FEPC [17] provides both feature extraction and pattern classification in a single run. This software allows the user to select different combinations of features to be extracted from a large group of images. Automatically, after feature extraction of all images, a combination of pattern classification methods selected by the user is implemented. However, in this research study, only the feature extraction application of this software was utilized to estimate the range of the values for each feature. The extracted feature values are recorded in a Text Document file type by the software. The results are imported to Microsoft Excel files for more data analysis and evaluation.

### 3.4.3 Microsoft Excel

Microsoft Excel is a spreadsheet application with several features such as calculation, graphing tools, and ranking which are applicable for this type of research study. All the graphs shown in this research study are provided by this software.

# CHAPTER 4

# METHODS AND PROCESSES

This research study utilizes four processes to investigate whether NIR imaging can be applied for maxillary sinusitis diagnosis. The processes, which are listed below, contain diverse image processing and data analysis methods.

- Data acquisition and image preprocessing
- Image segmentation
- Feature extraction
- Data analysis and classification

The experiments made by the processes, can be classified into two categories. In the first category, the processing applies to the images with their original histogram, however in the second category the color normalized images are used as inputs. The two categories of the experiments are represented in Figure 4.1 and Figure 4.2.

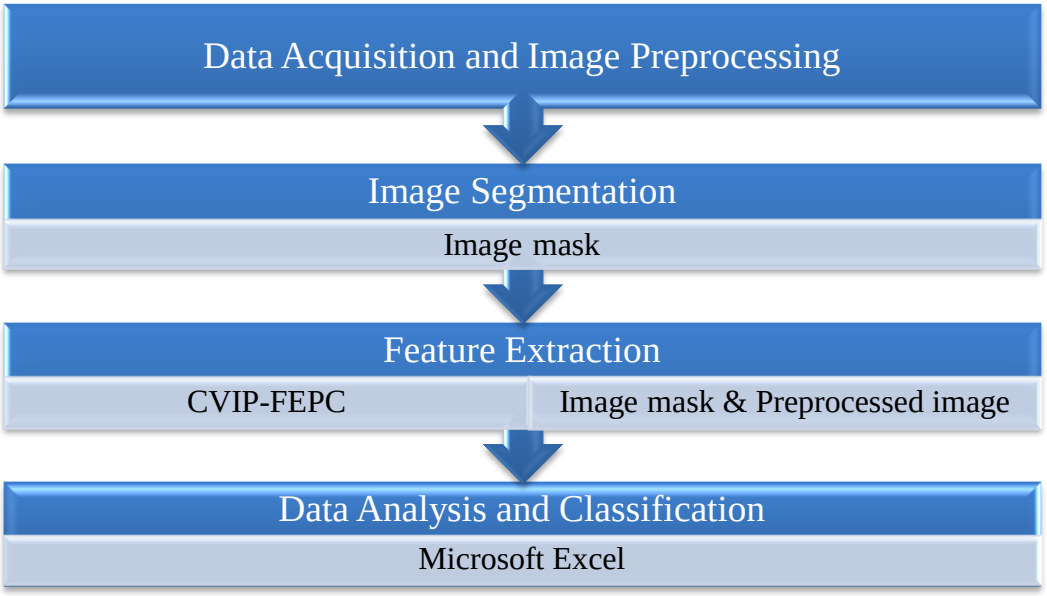


**Figure 4.1: First Category of Experiments Using Images with their Original Histogram**

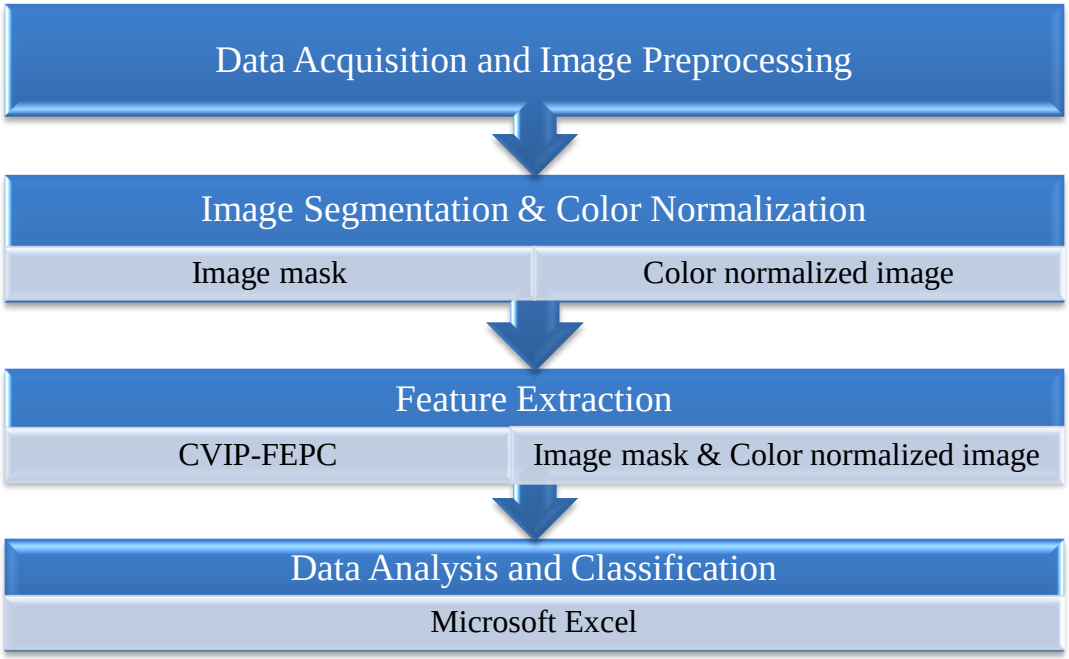


**Figure 4.2: Second Category of Experiments Using Color Normalized Images**

As it is illustrated in Figure 4.1, in the first category, the preprocessed images are applied directly in the feature extraction process. However, in the second category shown in Figure 4.2, the features of the color normalized images are extracted.

In the both categories, Figure 4.1 and Figure 4.2, the four main processes mentioned at the beginning are implemented by using same methods. This chapter is dedicated to describe the methods used in the four processes and also the color normalization method.

## 4.1 Data Acquisition and Image Preprocessing

The NIR images are captured from the subjects by a CCD camera in an examination room at the UC Irvine Medical Center. The CCD camera (the detector) is located on a height-adjustable tripod and approximately 10 inches in front the subjects with seated posture. The NIR light source is placed inside of the patient's mouth against the hard palate. In order to maintain sterility of the imaging procedure, the light source is covered by a new sanitary and disposable plastic bag for each subject, which is removed after each use. The NIR images are taken in the complete darkness with the least possible visible light in the room. This fact prevents saturation of the detector by the ambient visible light. The total imaging procedure takes approximately 60 seconds for each subject, during which several images from different perspectives are captured and then stored into a notebook PC.

Each of the recorded images is 4272×2848 pixels which uses approximately 2MB of the memory. This amount of memory usage becomes an important problem as it comes to processing and analysis of more than a hundred images. Therefore, a preprocessing step is applied to each and all the images before applying the main steps of image analysis. In this preprocessing step, each of the images is resized from 4272×2848 to 1024×512 pixels, to approximately 1/16 its

original size, by the decimation resizing method. This method simply eliminates the data by deleting rows and columns data with the factor of 1/4 in each dimension. Then, the resized images are saved as TIFF image format. All the images are resized and compressed by using CVIPtools software.

## 4.2 Image Segmentation

The preprocessed images will be subject to two image segmenting methods including mask creation and cropping. The data compression application of the image segmentation techniques is not negligible, especially in the image processing projects involving with a large amount of image data.

Mask creation is one of the image segmentation methods to partition a digital image into two types of segments with values of ‘0’ (black) and ‘1’ (white, in case of eight bits for each pixel the value is 255). In this study, the masks are created manually and as symmetric as possible between left and right sinuses for each image. The binary masks are simply applied on the preprocessed images by the math operation of multiplication. This process keeps the data of only a specific ROI (or a segment) and eliminates the unnecessary image data (Figure 3.5).

In order to reduce the memory and time needed to apply the created masks from maxillary sinuses area, the masks and their corresponding preprocessed images are cropped using the same coordinates. Therefore, the masks of the left and right sinuses are applied only on their corresponding segments cropped from the preprocessed images which are shown in (Figure 4.3).

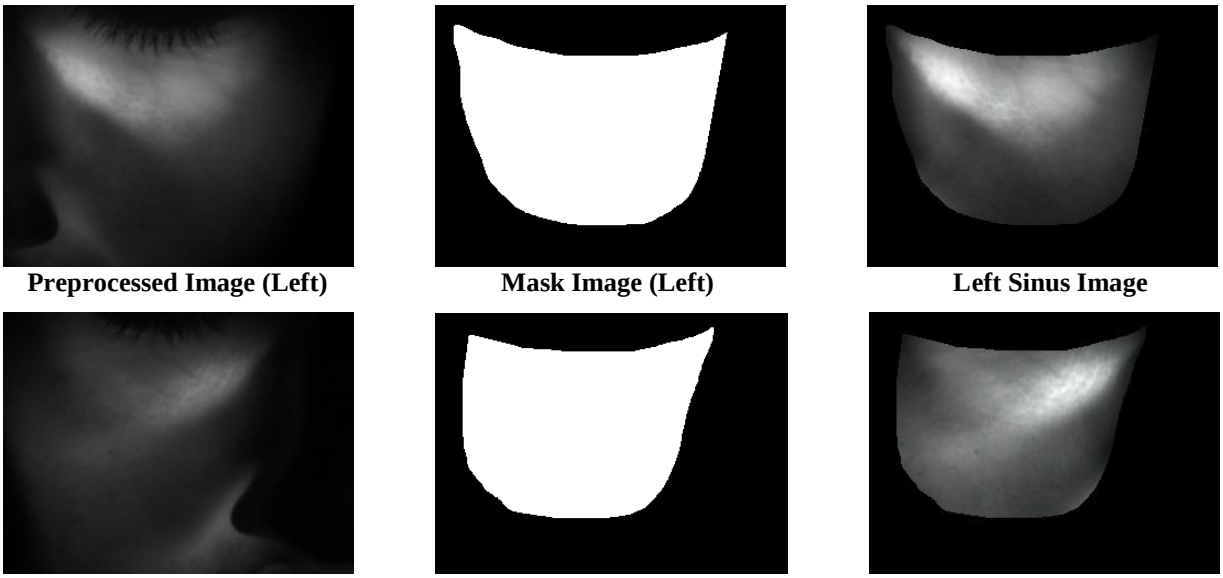


**Figure 4.3: Left and Right Maxillary Sinuses Regions after Segmentation**

## 4.3 Color Normalization

This research study investigates the diagnosis role of NIR images using their original color histogram and also color normalized histogram. Color normalization is applied to normalize the color histogram of each image in three dimensions of red, green, and blue.

Histogram stretch is the color normalization method applied on the images to rescale their histogram. As all the images have the data type of BYTE, the histogram stretch method rescales and stretches their histogram as the minimum data value moves to 0 and the maximum data value becomes 255. Figure 4.4 illustrates an image with its corresponding color histograms before and after histogram stretch. As it is shown in the Figure 4.4, by histogram stretching the contrast of the image is also increased.

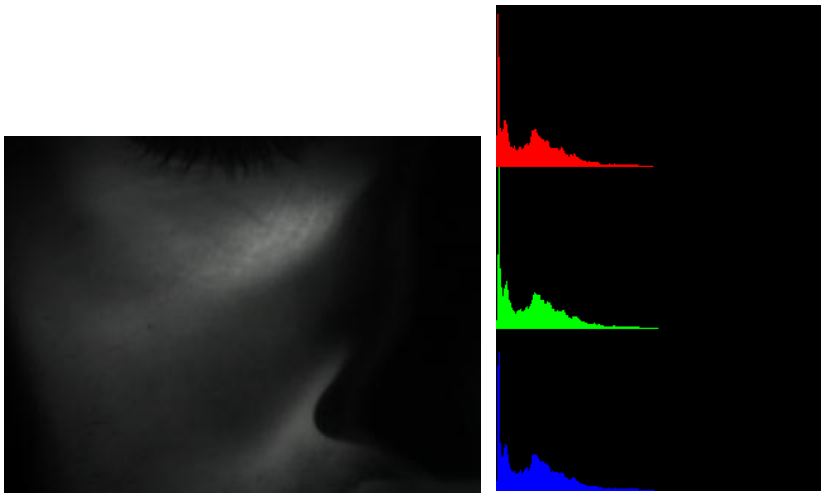

**(a) Sample Image before Histogram Stretch and its Color Histogram**

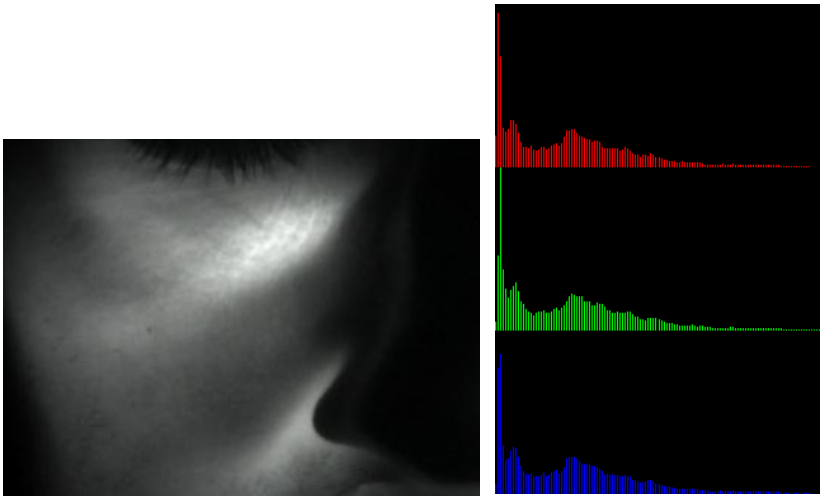

**(b) Sample Image after Histogram Stretch and its Color Histogram**

**Figure 4.4: Histogram Stretch Effect on a Sample Image and its Color Histogram**

## 4.4 Feature Extraction

The next process of the NIR image analysis is feature extraction. The input images of the CVIP-FEPC are can be either color normalized or original NIR images. In this process, several first-order and second-order features are extracted by the CVIP-FEPC application. These features include five types of histogram features, five types of texture features, and one type of spectral feature. The histogram features include histogram mean, standard deviation, skew, energy, and entropy. Also, the applied texture features are texture energy, inertia, correlation, inverse

difference, and entropy. The mentioned number for each feature represents only the number of different types of histogram, texture, and spectral features. However, in the real experiments of CVIP-FEPC, the total number of 46 features is extracted for each of the images. Since each histogram feature is extracted for three bands of red, green, and blue (RGB), the five types of histogram features would be in total 15 features. Also, for each type of texture feature (five types), the range and average of the four directions (will be explained in Section 4.4.2) are calculated which results in total 10 texture features. Moreover, the spectral feature is measured for three rings and three sectors. The spectral features of each sector and each ring are extracted for three color bands (RGB) which makes 18 spectral features. The number of 18 spectral features also should be added to three features of the spectral DC value for three color bands, so in total there are 21 spectral features. In this study, only histogram and spectral features of red band are utilized for data analysis. Since all of the three RGB channels include similar data, only the data of one the bands (red) is analyzed to prevent unnecessary computations.

### 4.4.1 Histogram Feature

The image histogram is a graphical representation of the number of pixels for each grey level value. In another word histogram is "a model of the probability distribution of the gray levels" [18]. The histogram features are statistical-based features which contain information about the grey-level distribution for the image. The histogram features are measured for three color bands of red, green, and blue (RGB) in case of using color images. Mean, standard deviation, skew, energy, and entropy are the features based on the first-order histogram probability.

The mean histogram feature is the average of the grey-level values, and the standard deviation feature describes the contrast of the image. The skew histogram calculates the asymmetry of the mean in the histogram. The energy of histogram is a maximum value of 1 for an image with a constant value and decreases as the number of grey-level values increase in the image. The histogram entropy measures the number of bits needed to code the data of each pixel [18].

### 4.4.2 Texture Features

Texture features can be measured by using the second-order histogram of the gray levels. The second-order histogram techniques are also referred as gray-level co-occurrence matrix or grey-level dependency matrix techniques which provide information about pairs of pixels and their related gray levels. Two parameters of distance and angle are necessary for texture features application. The distance refers to the pixel distance between the pairs of pixels, and the angle represents the angle between pixels in each pair [18]. In this study, the texture features are extracted based on a six pixel distance in each pair; then the average and the range of the texture features extracted in four directions are used for the next processes. The pixel distance value in texture features is dependent upon the scale of the regions of interest by pixel. The directions to be considered for the texture features are horizontal ($0^o$ and $180^o$), vertical ($90^o$ and $270^o$), left diagonal ($135^o$ and $315^o$), and right diagonal ($45^o$ and $225^o$), which are shown in Figure 4.5. Five texture features generated by the methods are provided by CVIP-FEPC, which are energy, inertia, correlation, inverse difference, and entropy.

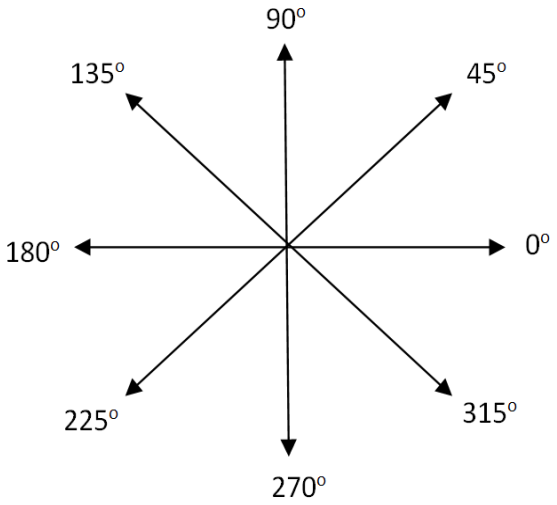


**Figure 4.5: Four Different Directions with Their Corresponding Angles**

The energy calculates the distribution across the grey level values which represents smoothness of the image. The inertia provides information about the contrast, while the correlation measures the similarities between pixels. The inverse difference calculates the homogeneity, and the entropy provides the information content which is inversely related to the energy [18].

### 4.4.3 Spectral Feature

Spectral features or frequency/sequency-domain based features are based on the power metric. The power can be calculated by the below formula which is the magnitude of the spectral components squared,

Where *T (u, v)* refers to any of the transforms, which the Fourier transform is typically used.

$$\text{Power} = |T\ (u, v)|^2$$

The standard spectral features are to extract the power of several spectral regions such as rings, sectors, or boxes. The spectral features can provide texture information of the image. The

regions with high power are related to the low frequency which represents coarse textures. As frequency gets higher, the power reduces and texture will be finer. In this research, the spectral feature is extracted from ring and sector regions with the parameter of three which is the number of the rings and sectors applied in the spectral domain based image [18].

### 4.5 Data Analysis and Classification

The extracted features from the images of left and right sinuses are subjects for data analysis and then classification. Therefore, 22 different features including histogram and spectral features extracted from red band and all the texture features are analyzed and classified. Since in most of the cases only one of the sinuses is affected by sinusitis, a feature-based asymmetry indicator is measured for each image as a key factor in sinusitis diagnosis. This metric may be a good potential to diagnose sinusitis based on the difference degree of the extracted features between left and right sinuses. The indicator is defined as follows,

$$A_i = \frac{F_{i,L} - F_{i,R}}{F_{i,L} + F_{i,R}}$$

$F_{i,L}$: Feature $i$ of left maxillary sinus

$F_{i,R}$: Feature $i$ of Right maxillary sinus

for $i = 1, 2, \ldots, 22$

It is expected to obtain $A_i$ value of about zero for the control images as their left and right sinuses are very similar in intensity and texture. However, non-zero values are achieved for sever images as they have obvious differences in left and right sinuses. In this study, we try to obtain the most efficient $A_i$ range of values for both control and sever images (train set). Next, the sensitivity and specificity are evaluated respectively by calculating the number of test images which match with the $A_i$ range of sever and control images.

Sensitivity and specificity are two success metric rates which are often used in biomedical image analysis with two classes of diseased and healthy. These measures can also be used in any object classification with a binary result. There are four definitions for this medical classification:

- True Positive (TP): sick person classified as sick correctly.
- False Positive (FP): healthy person classified as sick mistakenly.
- True Negative (TN): healthy person classified as healthy correctly.
- False Negative (FN): sick person classified as healthy mistakenly.

Then the sensitivity and specificity are defined as follows:

$$\text{Sensitivity} = \frac{number\ of\ True\ Positives}{number\ of\ True\ positives + number\ of\ False\ Positives}$$

$$\text{Specificity} = \frac{number\ of\ True\ Negatives}{number\ of\ True\ Negatives + number\ of\ False\ Positives}$$

# CHAPTER 5

# RESULTS AND DISCUSSIONS

The results of this research study can be categorized into three main sections which follow the research objectives. In the first section, the asymmetry indicator of the extracted features from control and sever classes are presented and compared. The second section is for the detection of sinusitis by using NIR images. Finally, in the last section, the investigation related to the effect of the image color normalization in sinusitis diagnosis is discussed based on the outputs.

## 5.1 Features Comparison between Control and Sever Classes

In this section, the feature-based asymmetry indicator defined in the previous chapter is measured from the training set images including control and sever classes. All the images have their original histogram and no color normalization is applied before the feature extraction. There are 22 graphs corresponding to 22 different features (see Section 4.4). Five graphs (Figure 5.1 through Figure 5.5) include the results related to five different histogram features. Also in Figure 5.6 to Figure 5.15, the results of the texture features are illustrated, and finally spectral features are shown in Figure 5.16 through Figure 5.22. In each graph, the horizontal axis illustrates the asymmetry indicator value and the other axis shows the number of images which is 65 for each class. The asymmetry indicator values related to each class are shown with different colors; control class with blue and sever class with red. This provides a good visual analysis of the extracted features for each class.

The first graph (Figure 5.1) shows the asymmetry indicator related to histogram mean of red band. Based on the results, all of the sever images have asymmetry indicator value more than 0.137, and the asymmetry indicator value related to control images are about less than 0.127. Since histogram mean feature separates control images from sever images without data overlapping, this feature is definitely selected as one of the discrimination factors for sinusitis diagnosis.

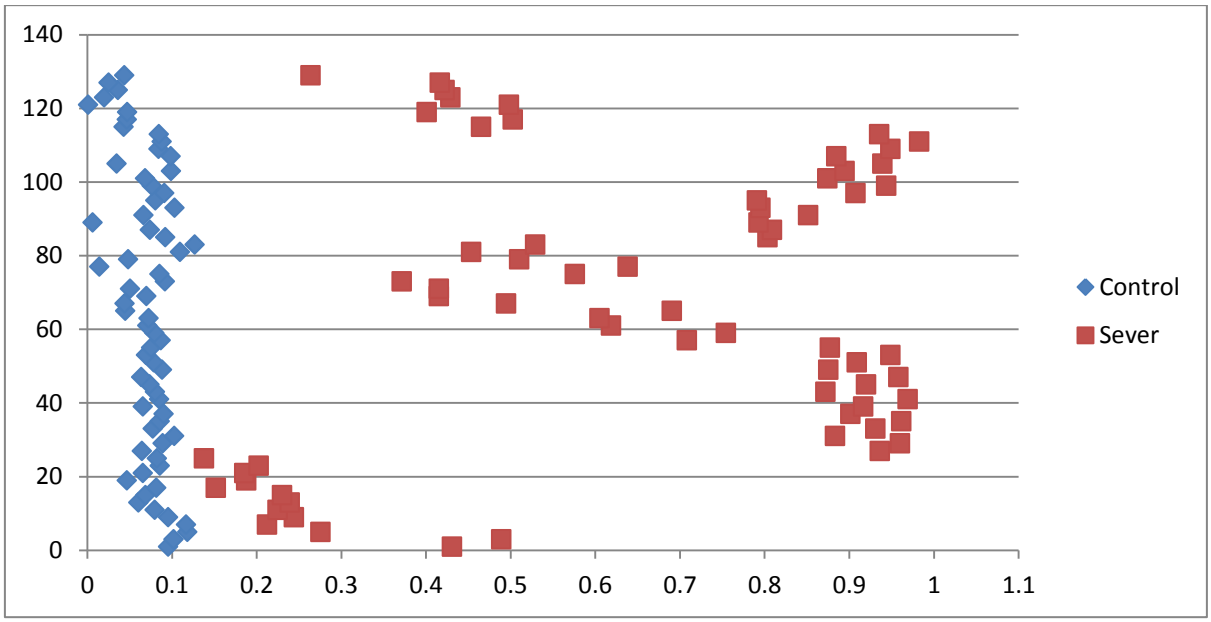


**Figure 5.1: Asymmetry Indicator of Histogram Mean Feature from Original Images**

As it is shown in Figure 5.2 to Figure 5.5, the rest of histogram features including standard deviation, skew, energy, and entropy are not able to categorize control class from sever class efficiently. In the mentioned histogram features, mostly there are overlapping of the data in the middle of the two classes which deny their role of data discrimination and thus disease detection.

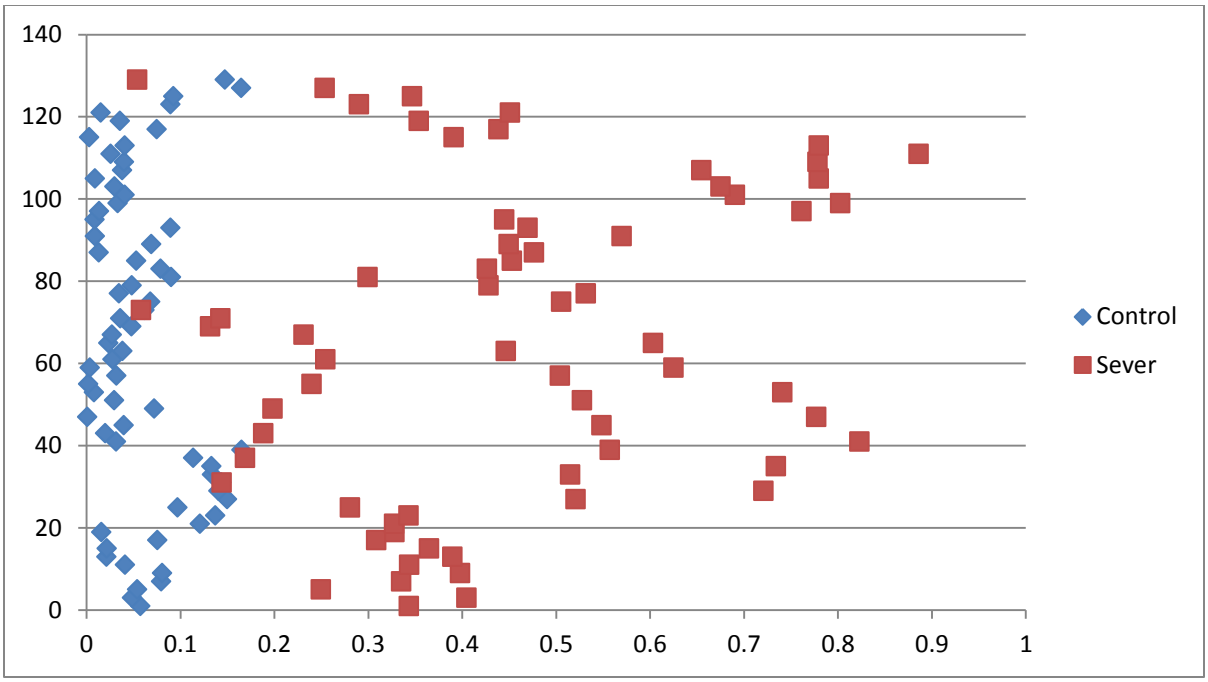


**Figure 5.2: Asymmetry Indicator of Histogram Standard Deviation Feature from Original Images**

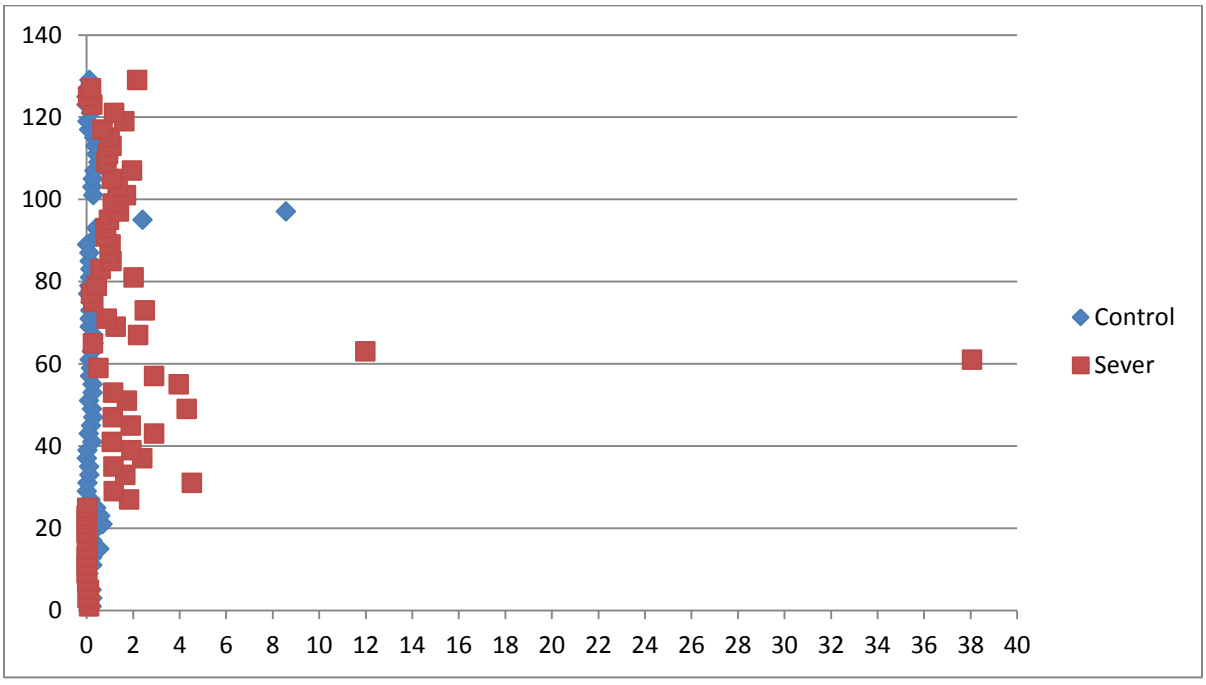


**Figure 5.3: Asymmetry Indicator of Histogram Skew Feature from Original Images**

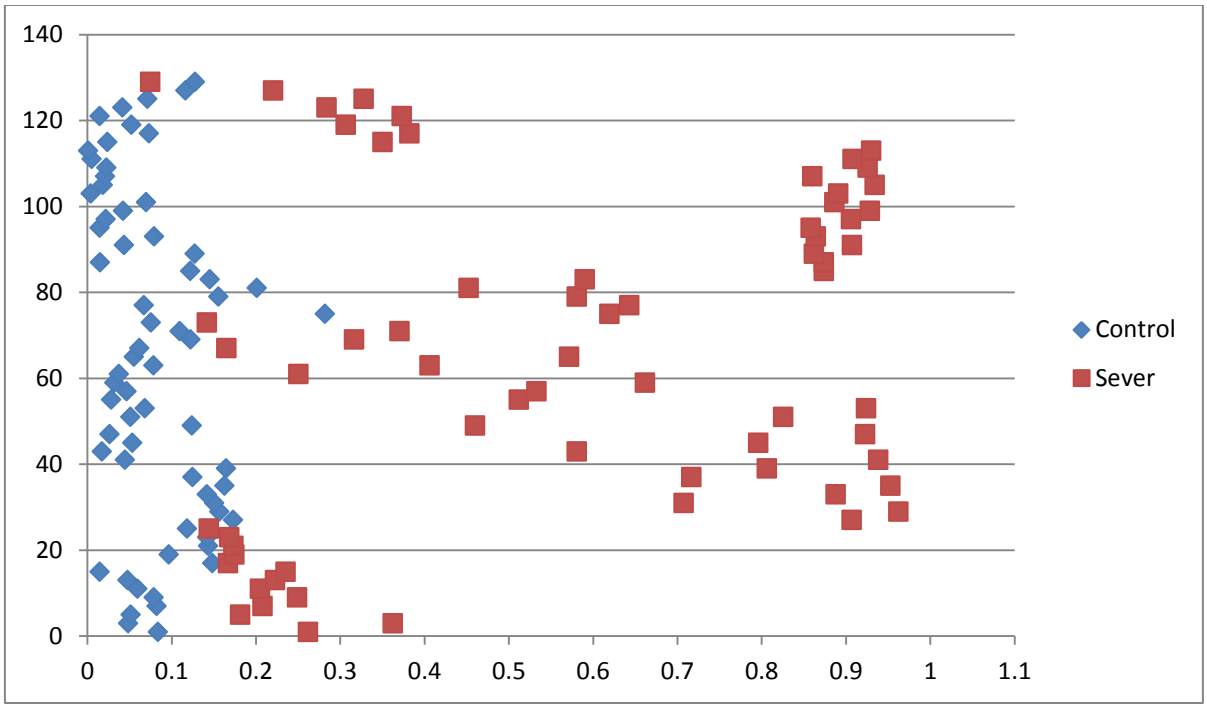


**Figure 5.4: Asymmetry Indicator of Histogram Energy Feature from Original Images**

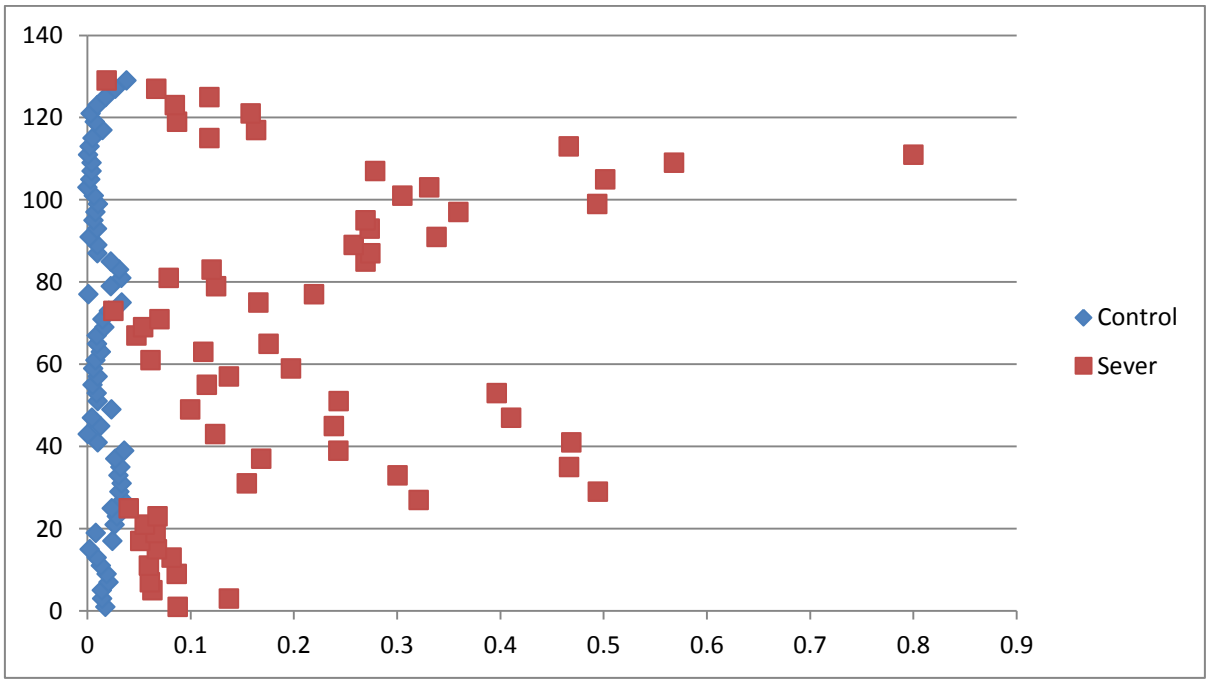


**Figure 5.5: Asymmetry Indicator of Histogram Entropy Feature from Original Images**

Among all the extracted texture features, texture inertia average (Figure 5.8) and entropy average (Figure 5.14) are selected to classify the test images and evaluate the NIR images potential to diagnose sinusitis. Although rest of the texture features categorize the two classes relatively, the overlapping data is still not negligible in comparison with the selected features. The following 10 graphs show the results obtained from the texture features.

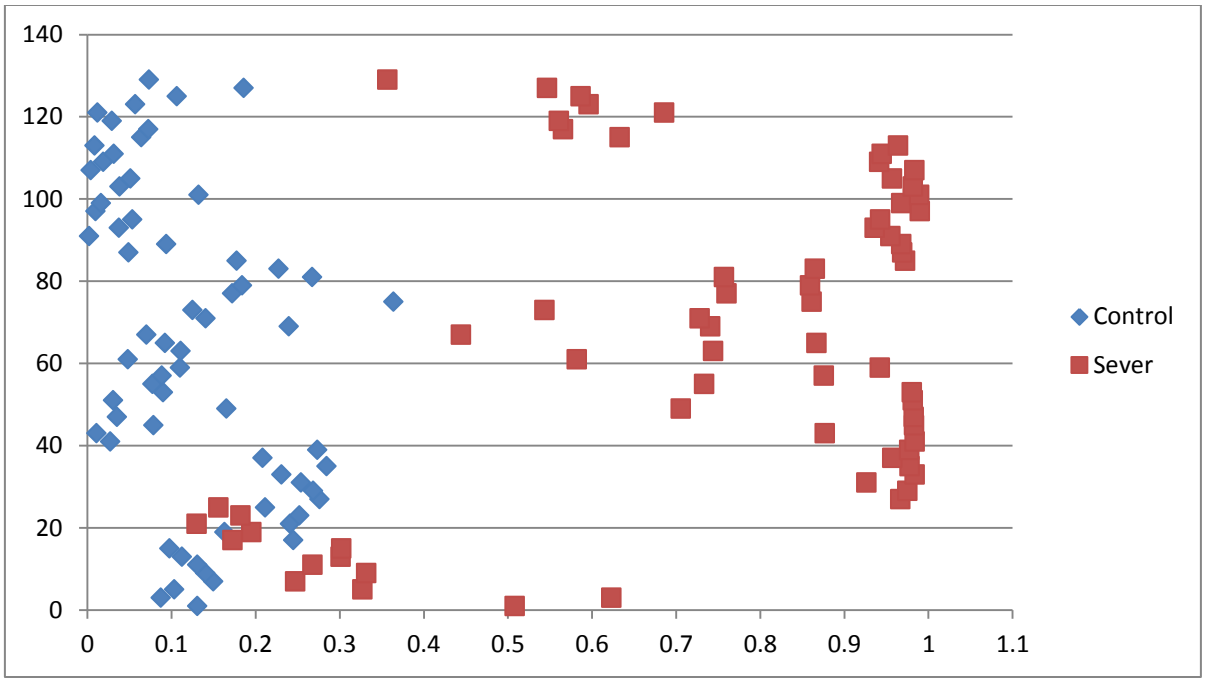


**Figure 5.6: Asymmetry Indicator of Texture Energy Average Feature from Original Images**

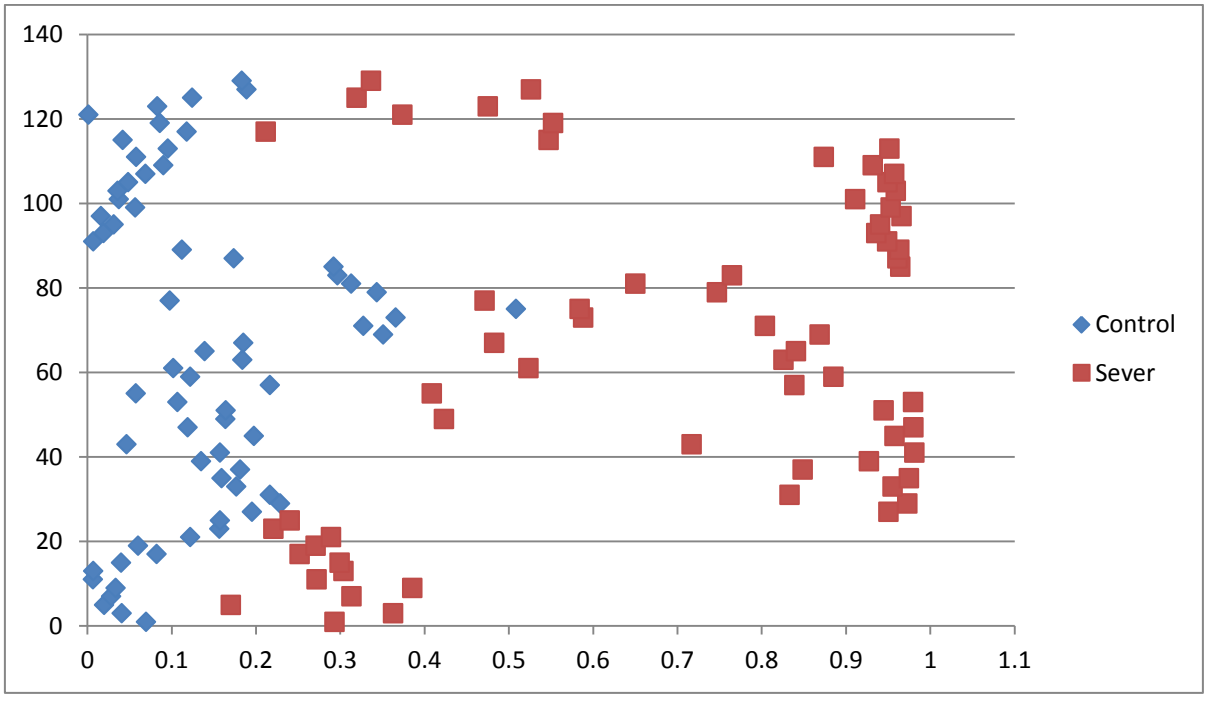


**Figure 5.7: Asymmetry Indicator of Texture Energy Range Feature from Original Images**

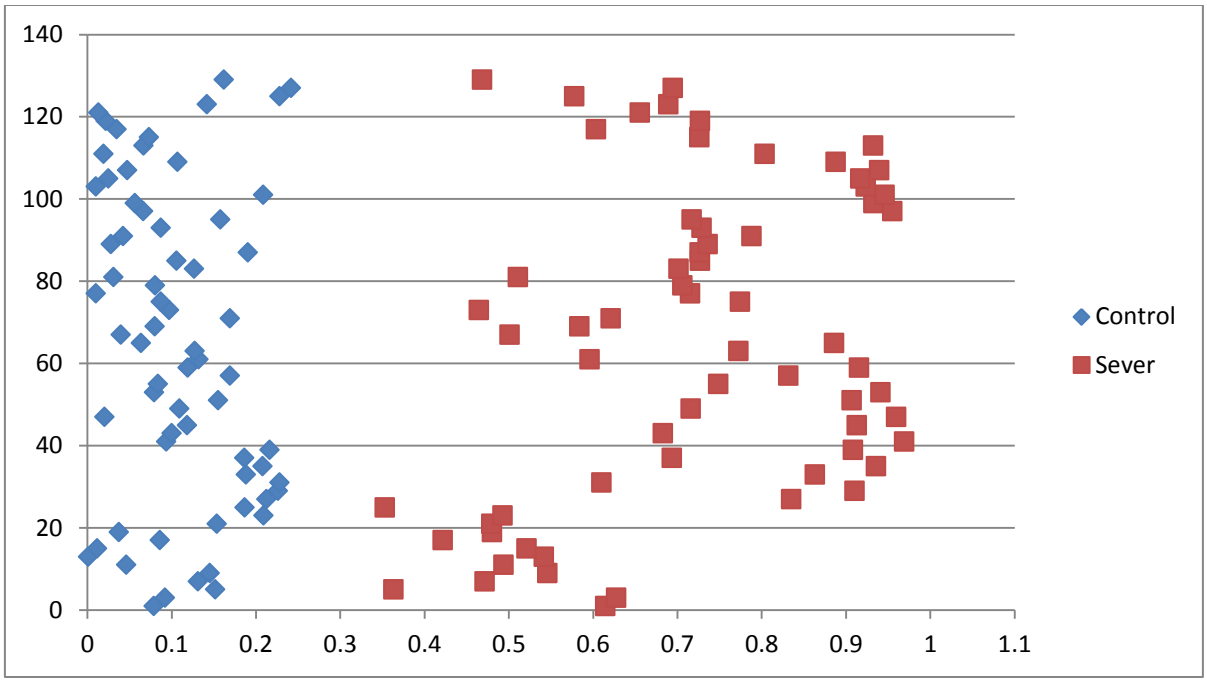


**Figure 5.8: Asymmetry Indicator of Texture Inertia Average Feature from Original Images**

The texture inertia (average) results in Figure 5.8 demonstrate the ability of this feature to classify control and sever classes. In these results, the lower boundary of the sever class is approximately 0.35, and the upper boundary for control class is 0.24. This means the two classes are discriminated perfectly with the separation distance of about 0.1. As the texture inertia average has a better functionality in the data classification than texture inertia range (Figure 5.9), the former is chosen for the test data analysis.

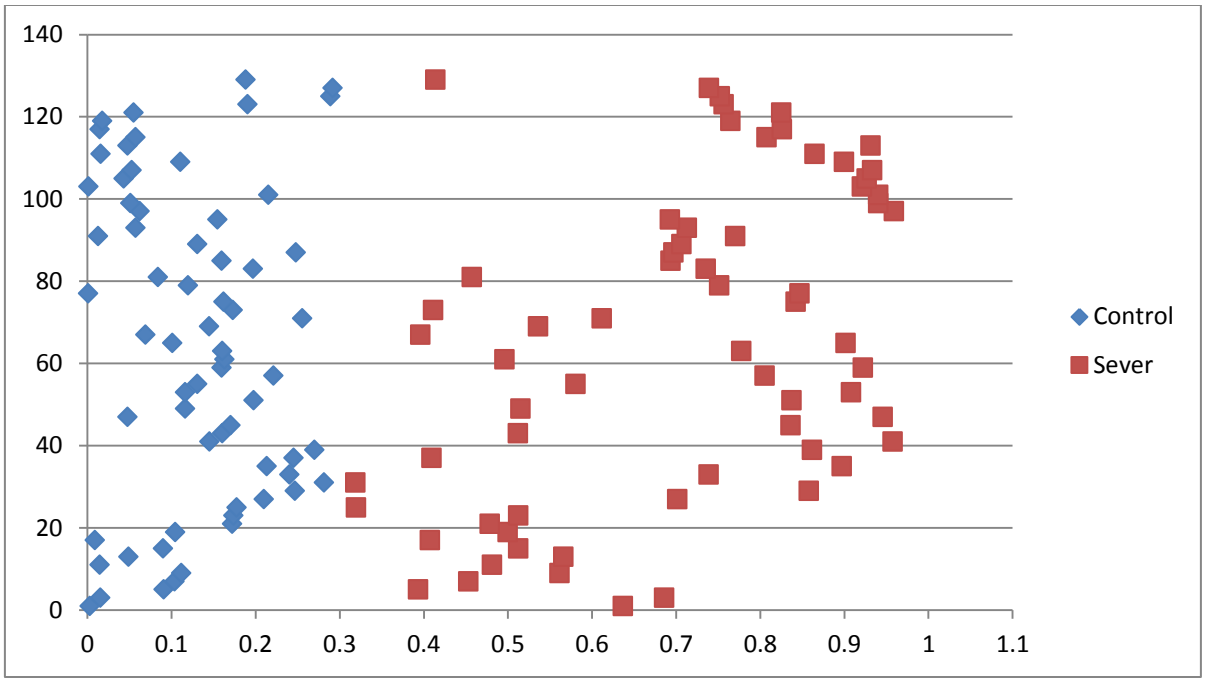


**Figure 5.9: Asymmetry Indicator of Texture Inertia Range Feature from Original Images**

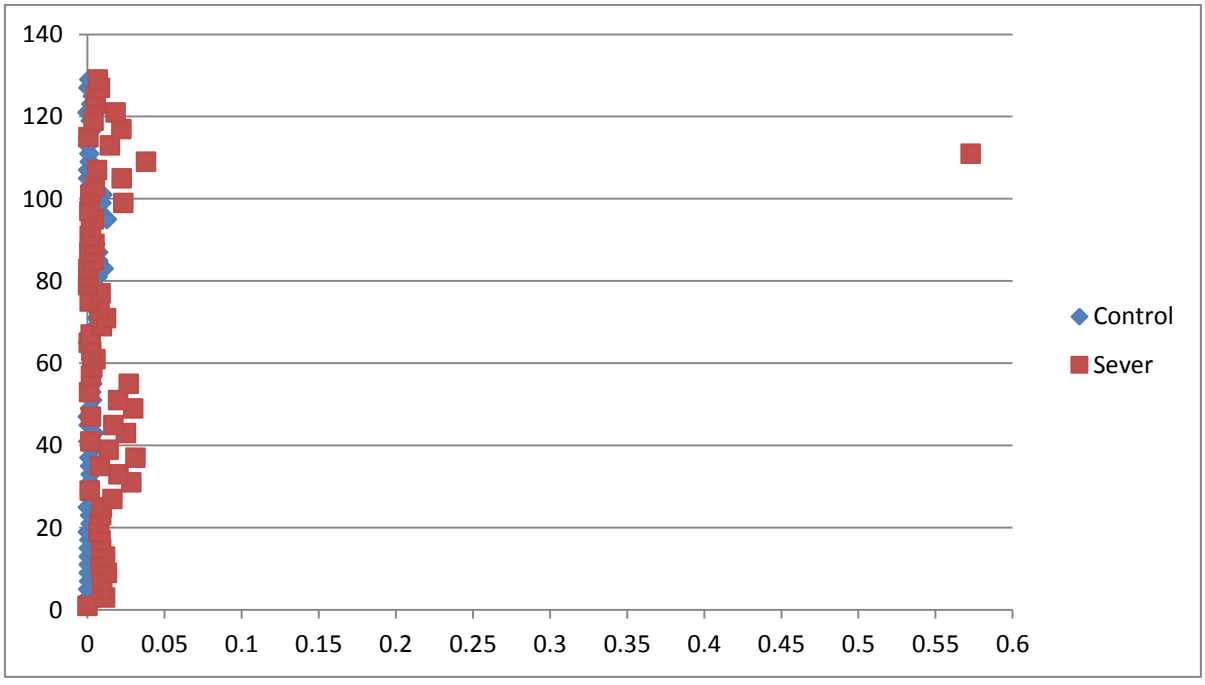


**Figure 5.10: Asymmetry Indicator of Texture Correlation Average Feature from Original Images**

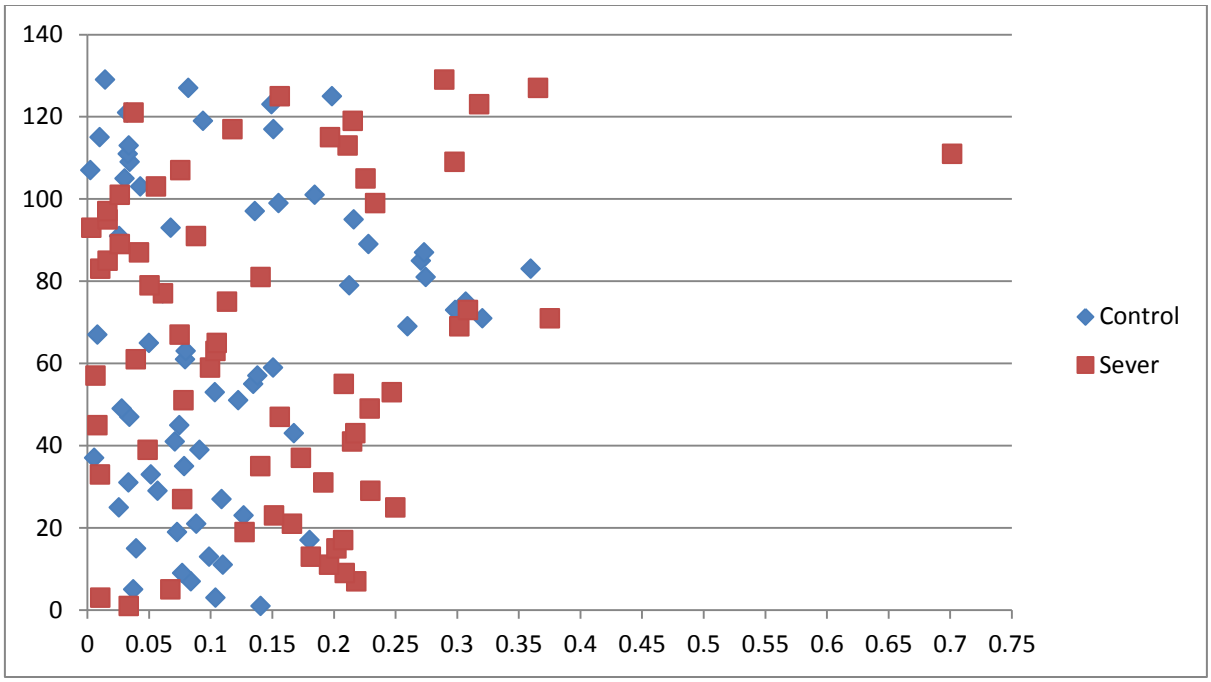


**Figure 5.11: Asymmetry Indicator of Texture Correlation Range Feature from Original Images**

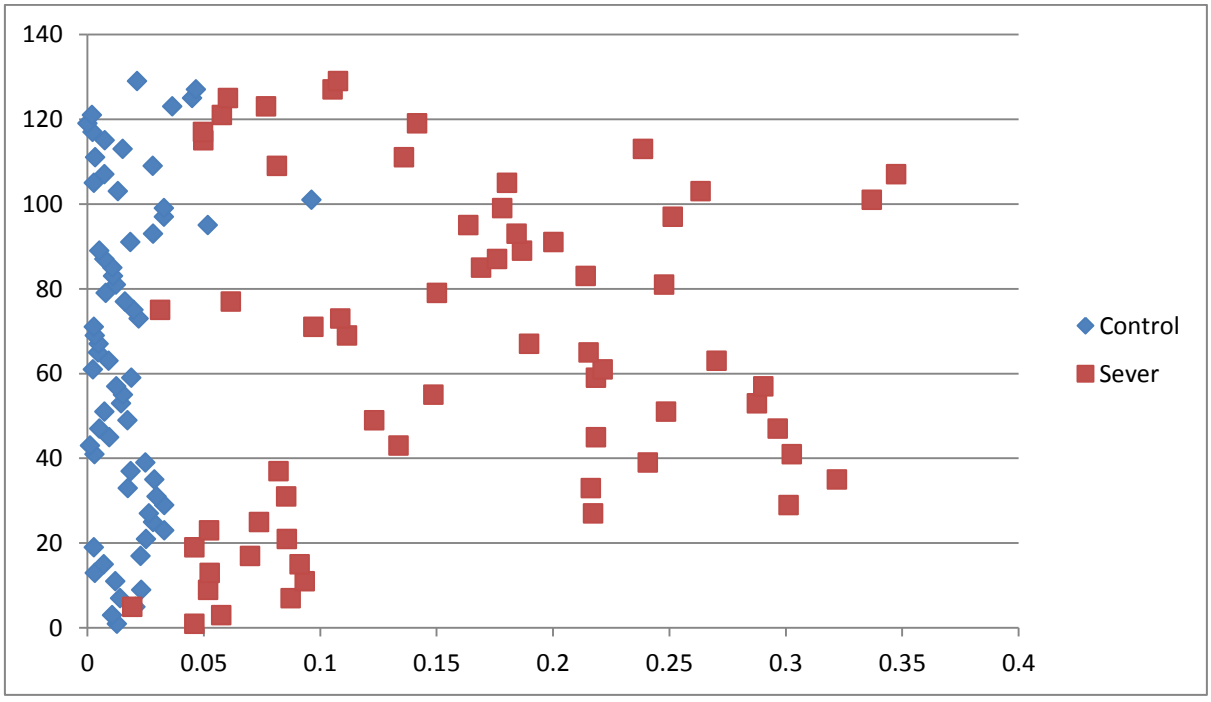


**Figure 5.12: Asymmetry Indicator of Texture Inverse Difference Average Feature from Original Images**

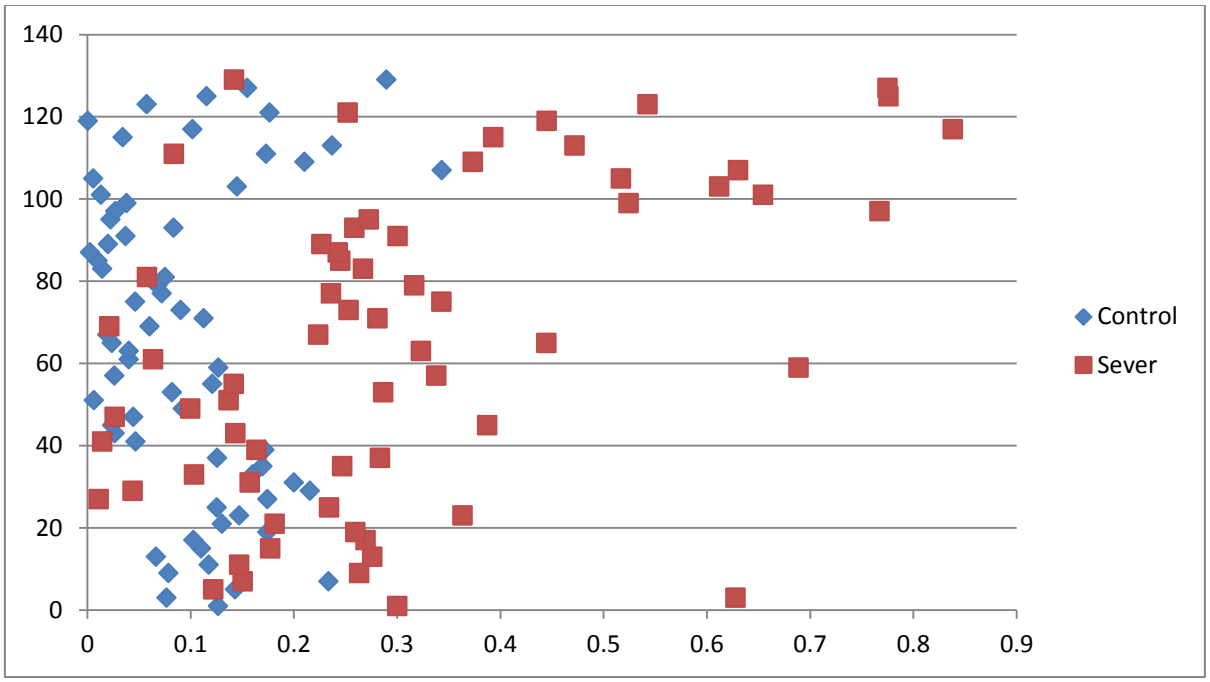


**Figure 5.13: Asymmetry Indicator of Texture Inverse Difference Range Feature from Original Images**

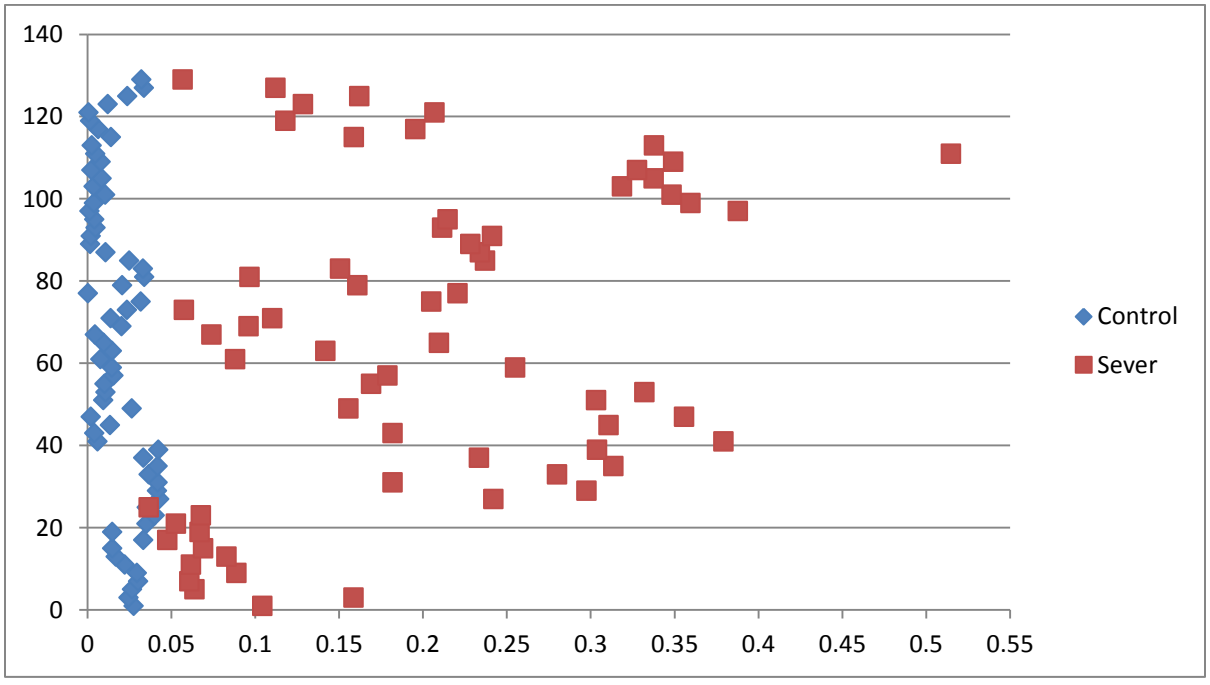


**Figure 5.14: Asymmetry Indicator of Texture Entropy Average Feature from Original Images**

Texture entropy average is the last feature which is picked for testing step. As you can see in Figure 5.14, the data for each class is categorized by this feature with the least amount of overlapped data of 0.02 (only one sever image out of 65). Except on the overlapped data, the rest of the data related to sever class are more than 0.047. Also, the control class data varies between 0 and 0.043.

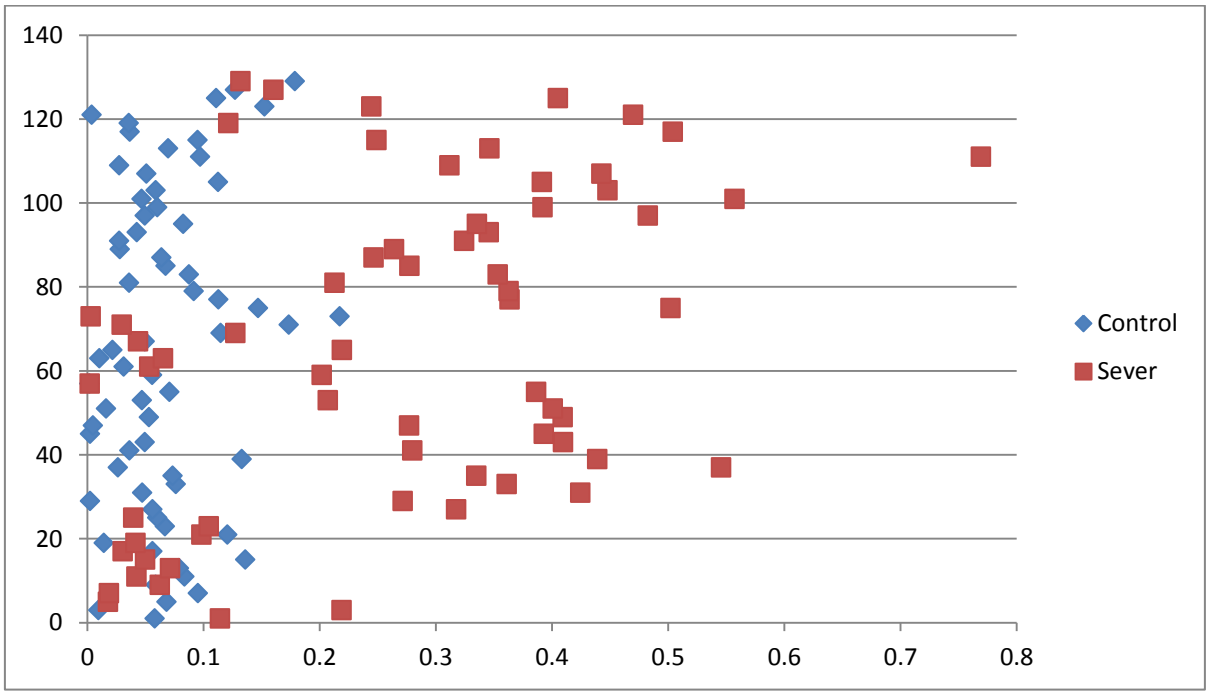


**Figure 5.15: Asymmetry Indicator of Texture Entropy Range Feature from Original Images**

The results related to the spectral features (frequency domain) are depicted in the last set of figures. As it is apparent in the following graphs, it is not possible to define a specific range of asymmetry indicator for each class, since the values of both classes are spread on all over the data domain. Therefore, it can be concluded that spectral features are not valid features for the purpose of sinusitis diagnosis using NIR images.

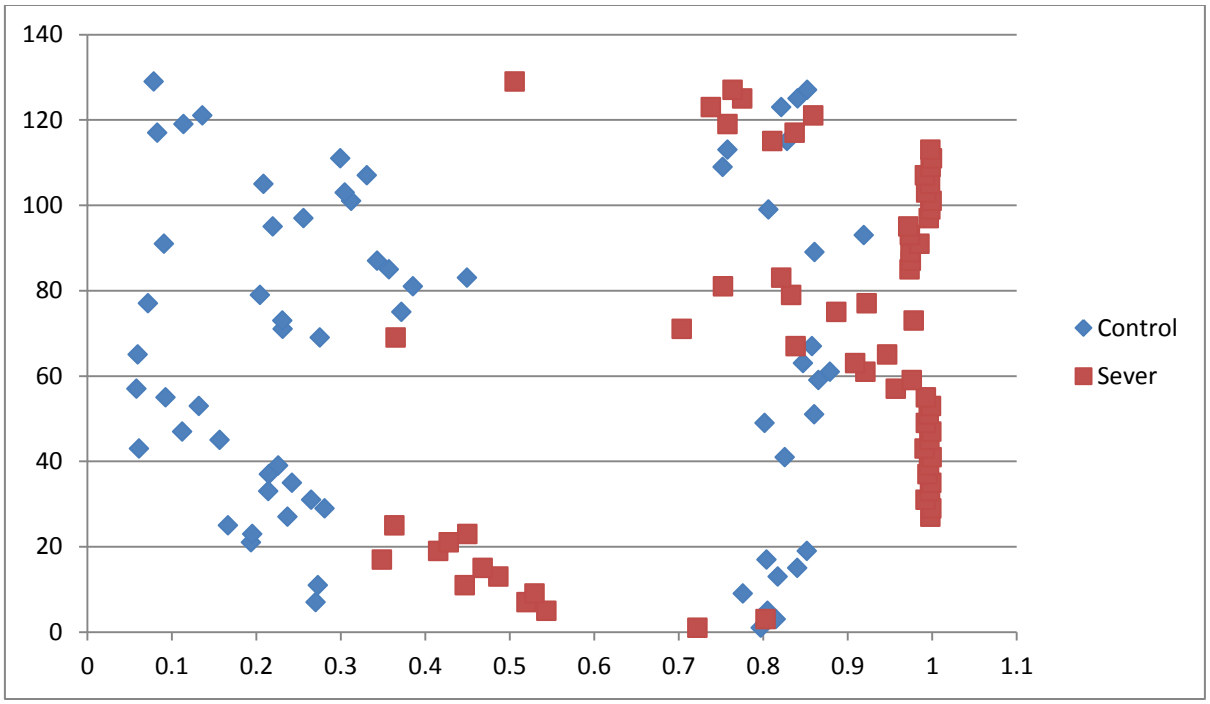


**Figure 5.16: Asymmetry Indicator of Spectral DC Feature from Original Images**

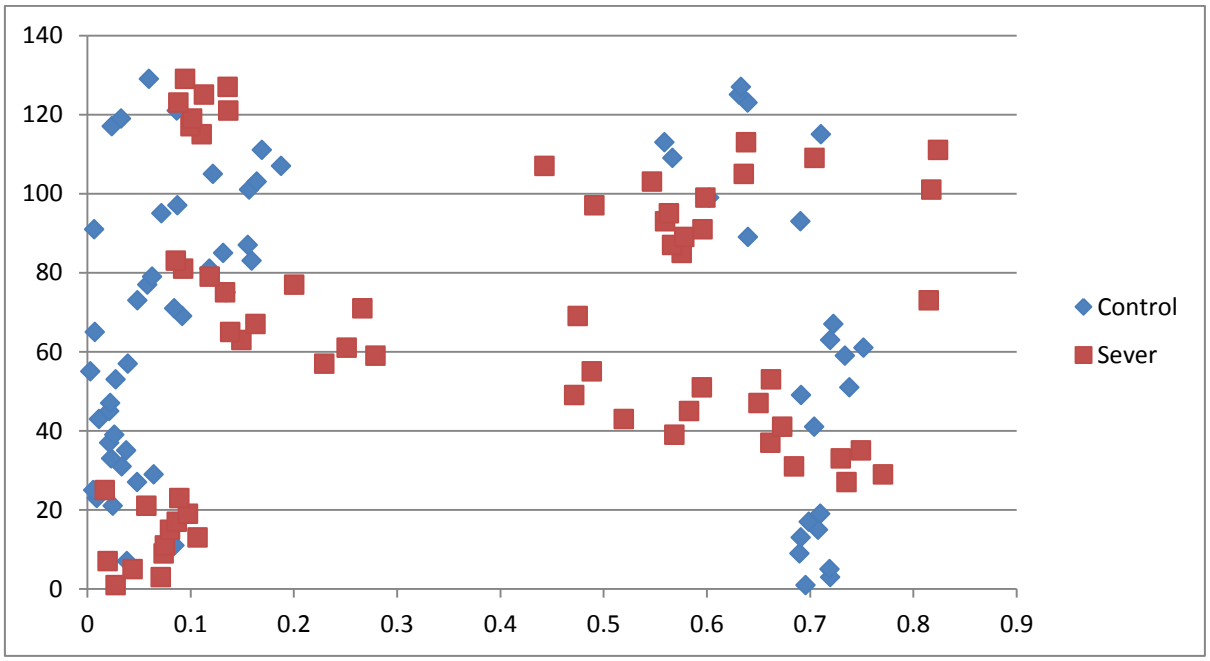


**Figure 5.17: Asymmetry Indicator of Spectral Ring1 Feature from Original Images**

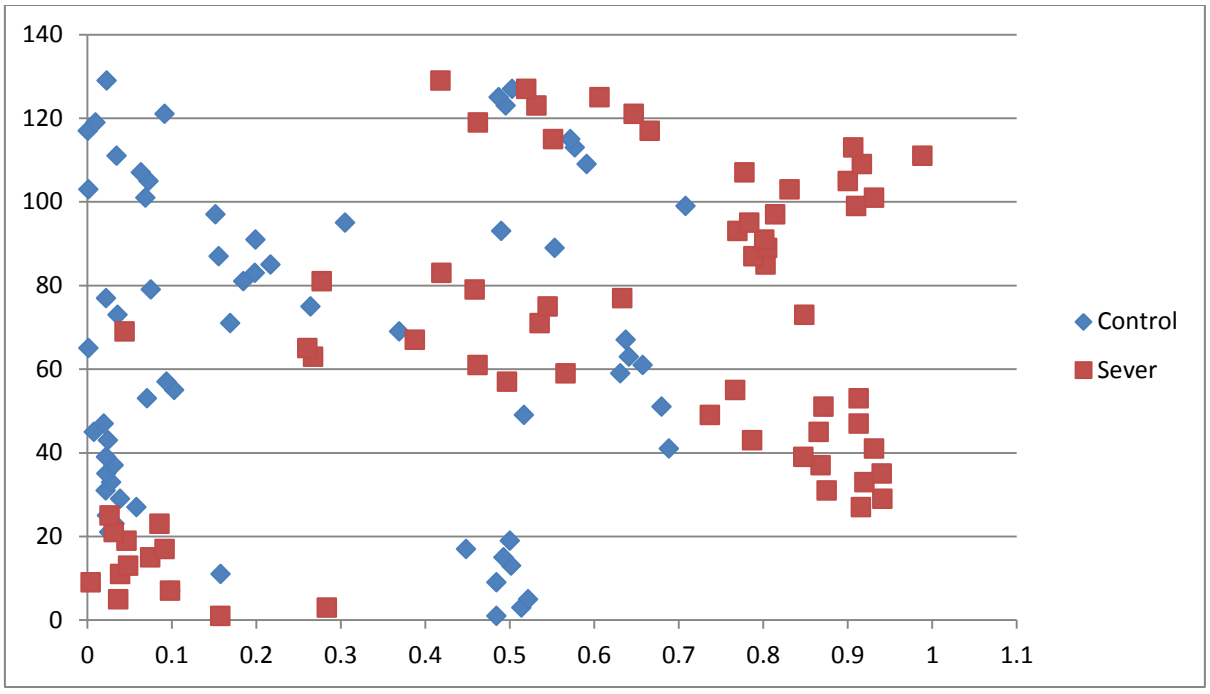


**Figure 5.18: Asymmetry Indicator of Spectral Ring2 Feature from Original Images**

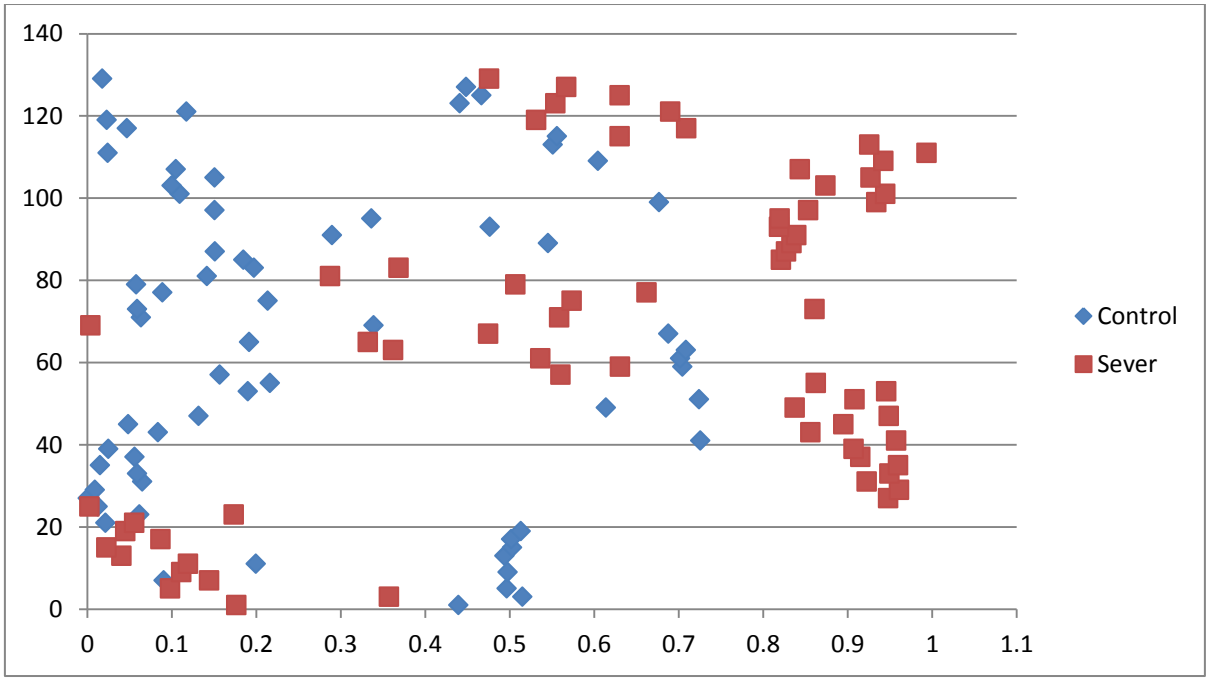


**Figure 5.19: Asymmetry Indicator of Spectral Ring3 Feature from Original Images**

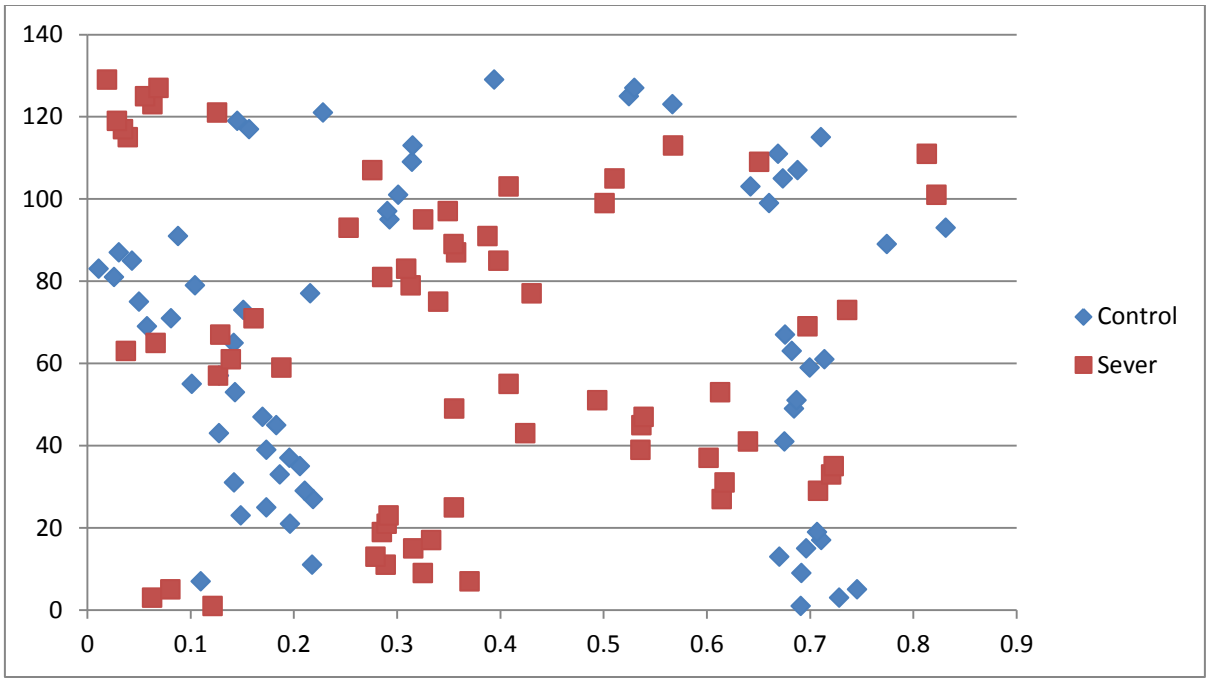


**Figure 5.20: Asymmetry Indicator of Spectral Sector1 Feature from Original Images**

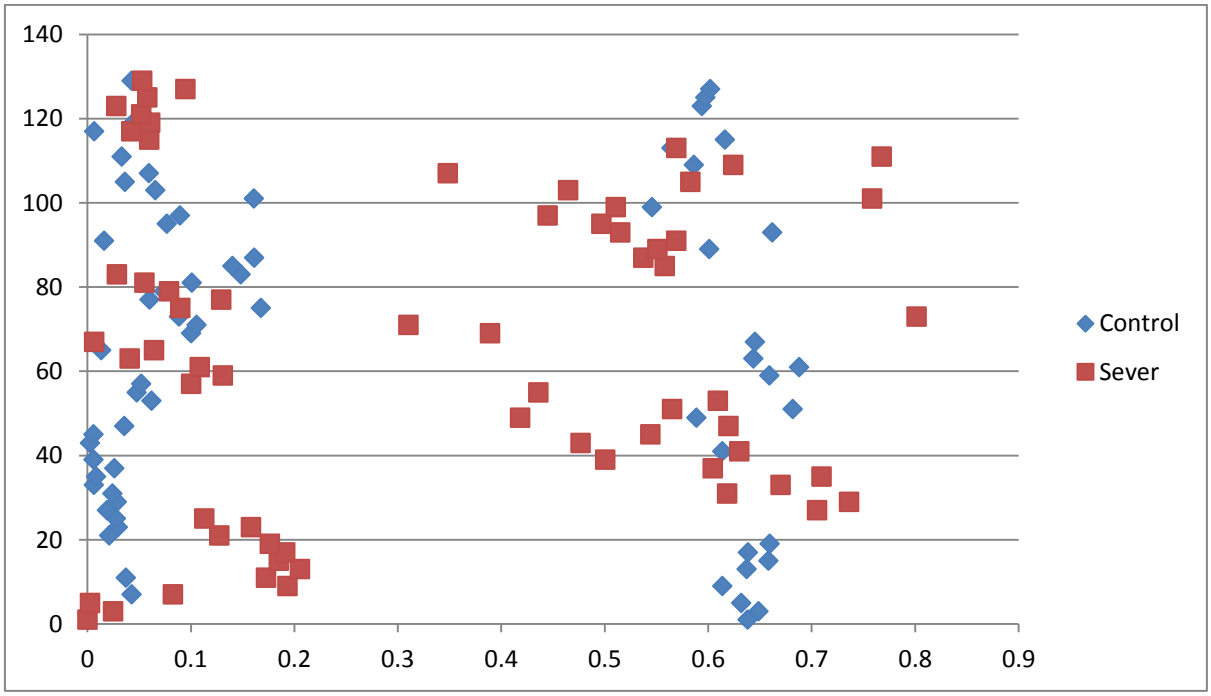


**Figure 5.21: Asymmetry Indicator of Spectral Sector2 Feature from Original Images**

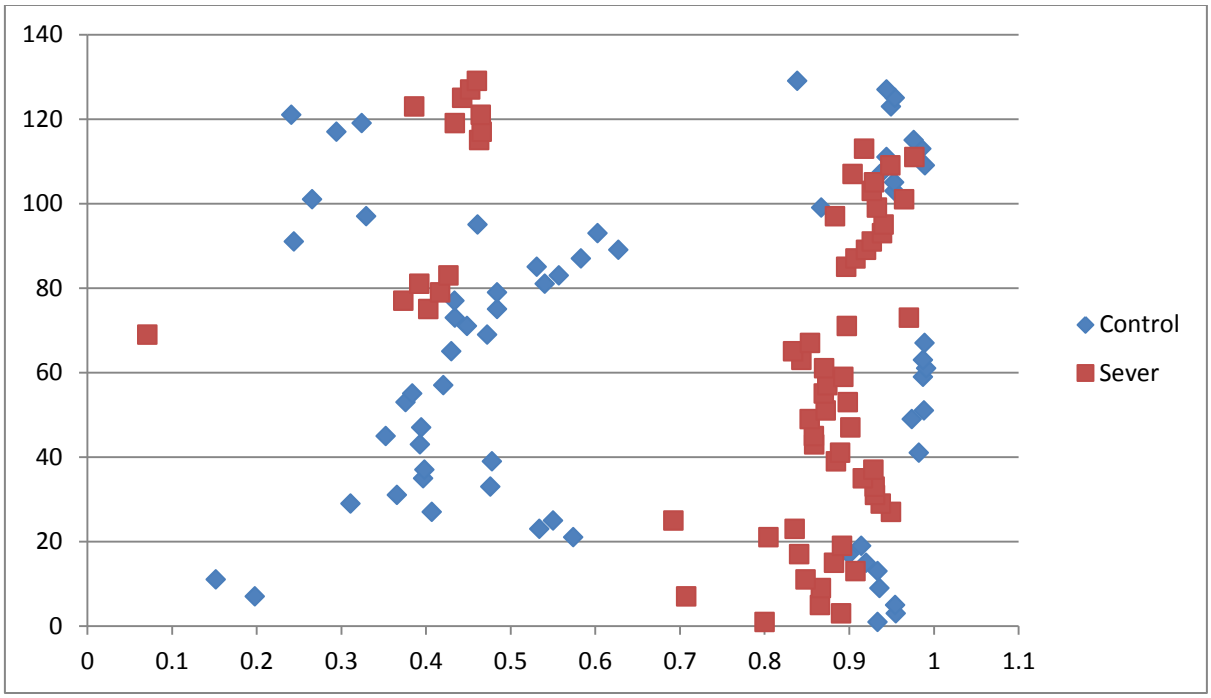


**Figure 5.22: Asymmetry Indicator of Spectral Sector3 Feature from Original Images**

Consequently, the best feature set to classify and analyze the NIR images of the test class includes histogram mean, texture inertia (average), and texture entropy (average) features. The asymmetry indicator range of values for control and sever classes related to each feature is mentioned in the Table **5.1**.

**Table 5.1: Asymmetry Indicator Range of Values for the Best Feature Set**

| **Feature Name** | **Asymmetry Indicator Range** | |
|---|---|---|
| | **Control Class** | **Sever Class** |
| Histogram Mean | (0- 0.127) | (0.137- 0.98) |
| Texture Inertia (average) | (0- 0.24) | (0.35- 0.97) |
| Texture Entropy (average) | (0- 0.043) | (0.047- 0.51) |

## 5.2 Sinusitis Detection

In this step, the test images are analyzed based on the data obtained from the training set. The selected texture set is extracted from the test images, and their asymmetry indicators are compared to the data range related to sever and control classes (Table **5.1**). The percentage of the test class normal images fitting within the range of the training set control images is the specificity of the analysis. Also, the sensitivity is the percentage of the test class abnormal images which matches within the range of sever images in the training set.

The following graphs show the asymmetry indicator values related to the three selected textures extracted from the normal and abnormal images in the test class. The first graph depicts the results obtained from histogram mean feature (Figure 5.23).

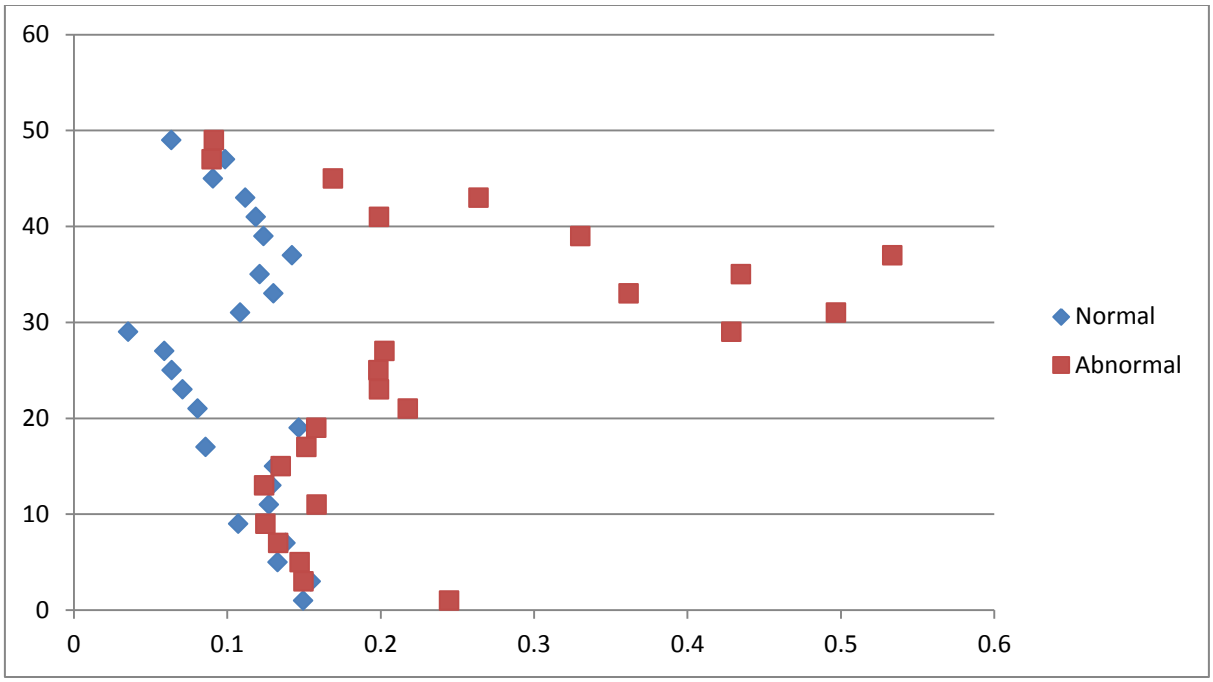


**Figure 5.23: Asymmetry Indicator of Histogram Mean Feature from Test Images**

According to the results illustrated in Figure 5.23, the asymmetry indicator of 16 out of 25 normal images fit into the training set range of values of control images (0- 0.127). Therefore, the specificity value obtained by histogram mean feature is 64%. The sensitivity value is also measured by counting the number of abnormal images which have the asymmetry indicator values more than 0.137, which results is a sensitivity value of 76%. As there is a gap of data between the data ranges corresponding to the control and sever classes (see Table **5.1**), the testing results fall in this gap are potential mild sinusitis cases and subjects to being scanned by the CT scanner. Based on the testing results obtained by the histogram mean feature, 28% of the test cases fall in this gap including 20% normal images and 8% abnormal images. The second feature which is analyzed in the testing step is texture inertia average exposed in Figure 5.24.

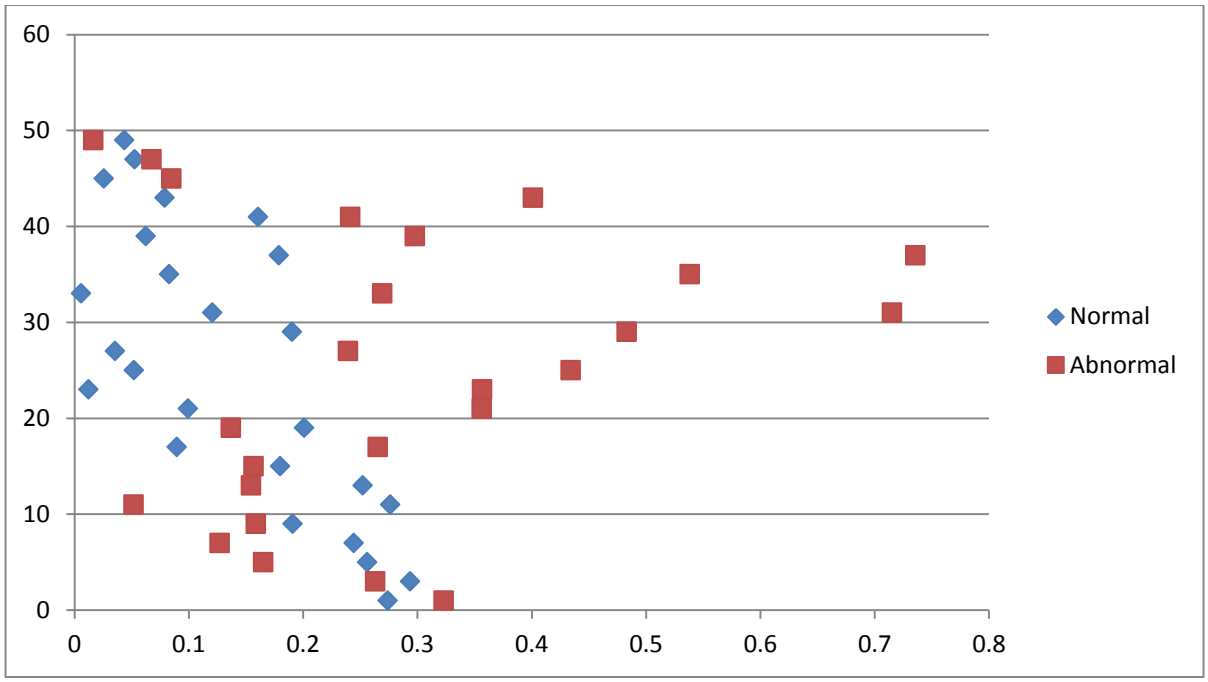


**Figure 5.24: Asymmetry Indicator of Texture Inertia Average Feature from Test Images**

As it is illustrated in Figure 5.24, the specificity value measured from texture inertia average results is 76%. However, the sensitivity of this feature to diagnose sinusitis is as low as 32%. 48% of the whole data including normal and abnormal images equally (24% of each of them) is within the gap between the data ranges corresponding to the control and sever classes. The following graph is texture entropy average results shown in Figure 5.25.

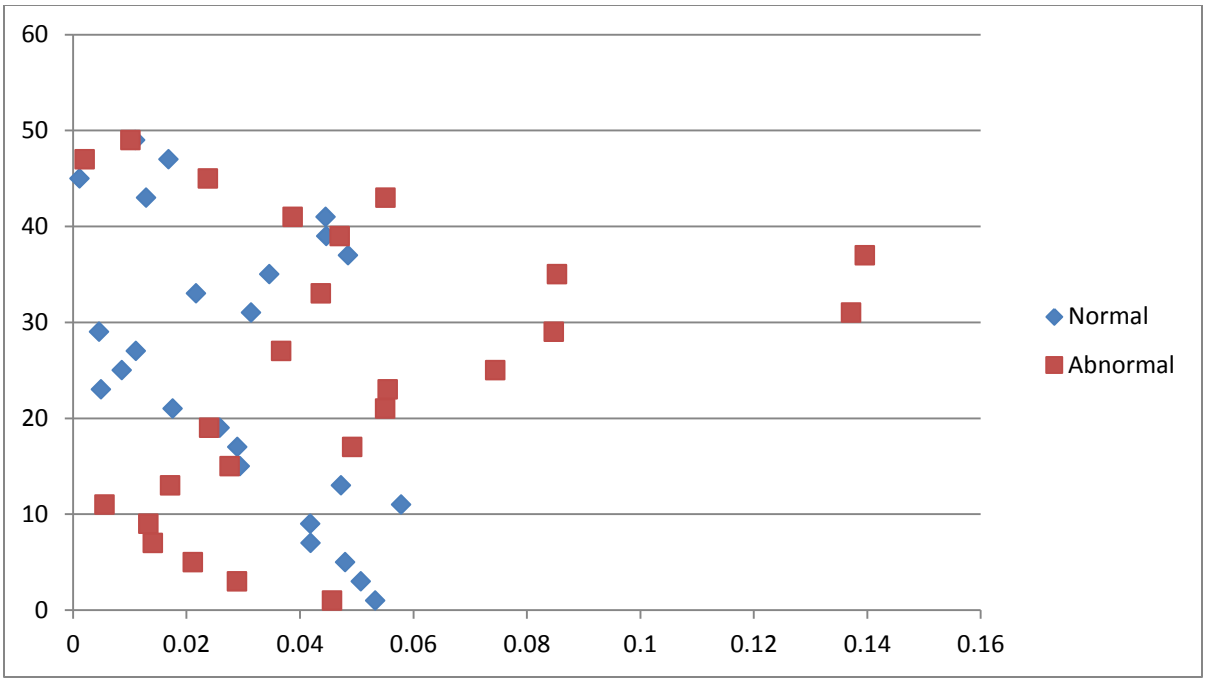


**Figure 5.25: Asymmetry Indicator of Texture Entropy Average Feature from Test Images**

Based on the texture entropy results and the training set data range, the specificity and sensitivity are measured which are 68% and 40%, respectively. Also 8% of each of the abnormal and normal data is in the gap between the data ranges of sever and control classes.

Consequently, the overall results of the three features in sinusitis diagnosis are summarized in Table 5.2. In this table, the data of training set is categorized by three colors for each data range. Green color means the control range of data and red is the data range of the sever class. Also yellow is defined as the data gap between the two former ranges of data, which is expected to include mild sinusitis cases.

**Table 5.2: Summary of Testing Results based on the Training Ranges of Values**

| | Histogram Mean | | | Texture Inertia | | | Texture Entropy | | |
|---|---|---|---|---|---|---|---|---|---|
| | | | | | | | | | |

| | | | | | | | | | |
|---|---|---|---|---|---|---|---|---|---|
| Normal | **16/25** | 5/25 | 4/25 | **19/25** | 6/25 | 0/25 | **17/25** | 2/25 | 6/25 |
| Abnormal | 4/25 | 2/25 | **19/25** | 11/25 | 6/25 | **8/25** | 13/25 | 2/25 | **10/25** |

As it is shown in Table 5.2, histogram mean and texture inertia include the highest sensitivity and specificity of 76%, respectively. Also, most of the features specificity results are higher than their sensitivity.

## 5.3 Image Color Normalization Effect in Sinusitis Diagnosis

This section of the experiments is to investigate whether the color normalization of the NIR images improves the sinusitis detection. In order to determine the effect of the color normalization on the NIR images, the best feature set selected from the original images are extracted from the color normalized images. The asymmetry indicator related to each feature is calculated and results in the following graphs of data. Figures below illustrate the asymmetry indicator of normalized images measured from the three selected features. The features include histogram mean, texture inertia average, and texture entropy average. Figure 5.26 shows the data corresponding to the histogram mean feature which is extracted from color normalized images.

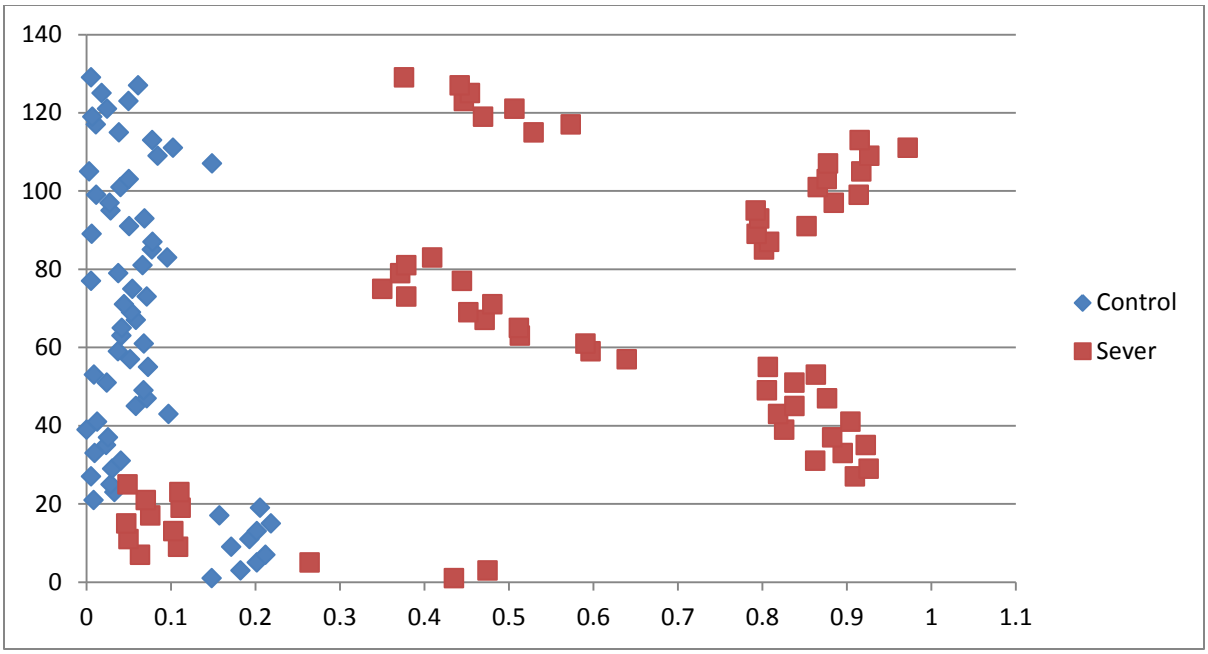


**Figure 5.26: Asymmetry Indicator of Histogram Mean Feature from Normalized Images**

By comparison of the results obtained from color normalized images to the similar results from original images, it is concluded that the discrimination functionality of the selected feature set to classify control and sever classes is degraded by color normalization. Similar results are gained for the other two features. As you can see in Figure 5.27 and Figure 5.28, not only color normalization doesn't improve the classification role of the features, but also it increases the amount of overlapped data between the control and sever classes. Therefore, color normalized images don't result in better range of values for each class than the original images. Consequently, testing step is denied to be applied on the training data collected from normalized images.

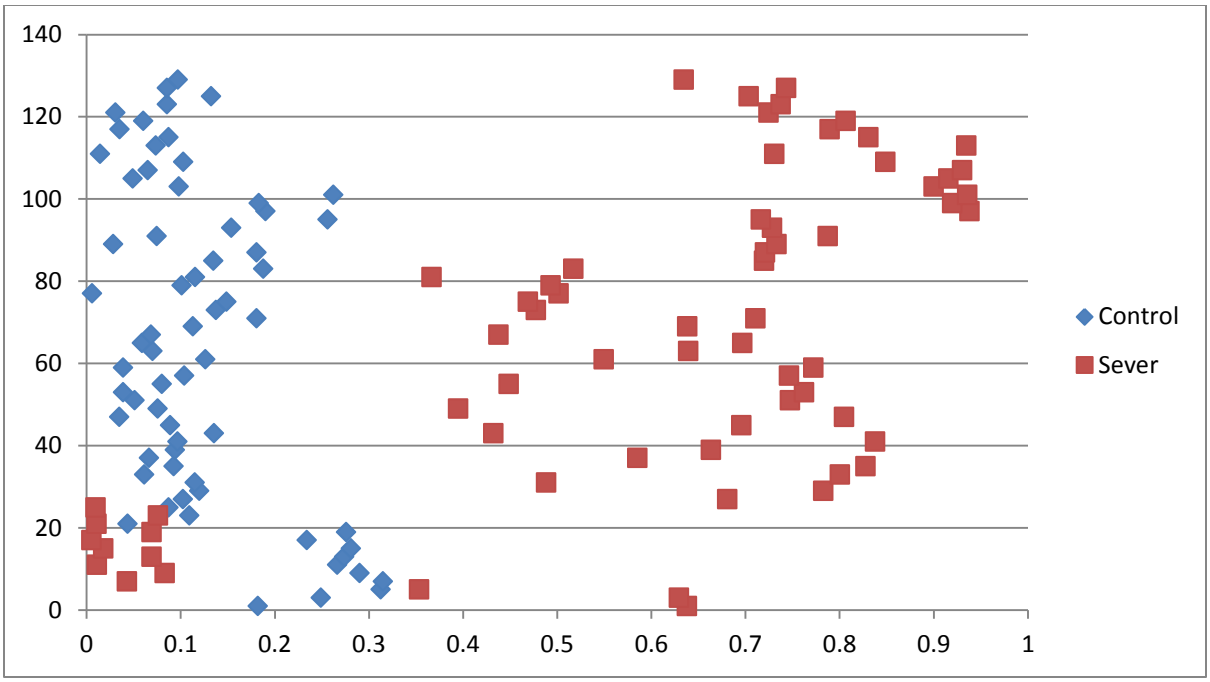


**Figure 5.27: Asymmetry Indicator of Texture Inertia Average Feature from Normalized Images**

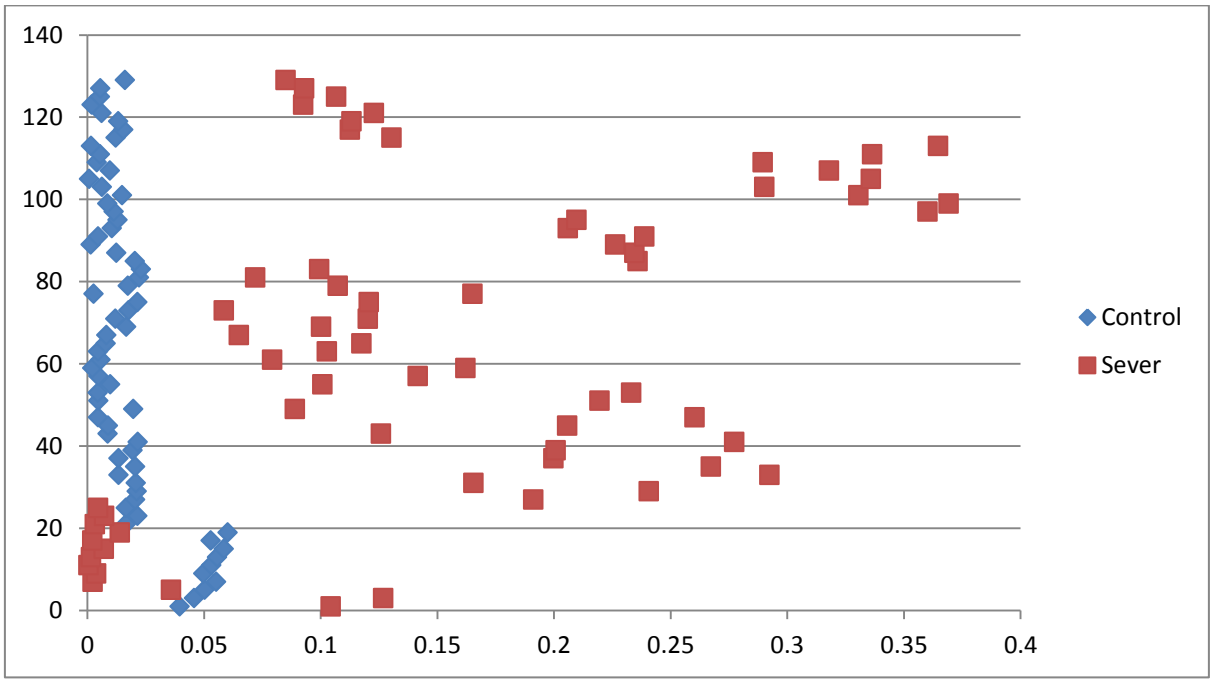


**Figure 5.28: Asymmetry Indicator of Texture Entropy Average Feature from Normalized Images**

# CHAPTER 6

# CONCLUSION

The research study is to determine if it is possible to diagnose sinusitis by NIR image analysis. Based on the conditions under which the study was performed, the answer is by the sensitivity value of 76% from histogram mean feature, it is possible to detect canine sinusitis with the NIR images.

Among all the features extracted from the NIR images histogram mean, texture inertia average, and texture entropy average are more efficient in data discrimination of control and sever classes. However in the testing step the obtained results are not reliable for sinusitis diagnosis. The first feature, histogram mean outcomes the most efficient results among all other features; sensitivity value of 76% and specificity of 64%. Secondly, texture inertia average makes sensitivity of 32% and specificity of 76% which denies its potential to detect abnormal cases. The last feature is texture entropy which produces sensitivity of 40% and specificity of 68%. Therefore, it is not possible to rely on the results obtained by the last feature too. Most of the features result in higher specificity values than the sensitivity values which lead to decrease unnecessary CT scans for normal cases. Although the absolute sensitivity of the features are not high enough, the number of abnormal images in the yellow region helps to improve the number of correctly diagnosed images. As the images in the yellow region are considered as mild sinusitis cases, they are subject to being analyzed in more detailed by gold standard CT scanners.

In this study, also we tried to determine whether the color normalization of the NIR images can influence on the results and also in the disease diagnosis. According to the extracted features data collected from color normalized images, color normalization degrades the discrimination

ability of the features in the training set. Therefore, testing step is not recommended to be implemented based on the worse training data.

# CHAPTER 7

# FUTURE SCOPE

In this research study, the NIR images are taken from few numbers of patients and normal cases. If the number of NIR images used in the experiments is increased, the results and conclusion based on them should be more reliable. Also the final results are measured for each feature separately. This step also can be done by using linear or nonlinear discriminant analysis algorithms in which the data classification is implemented in a three dimension data space based on all of the three features.

# REFERENCES

1- Margaret J. Fehrenbach, Susan W. Herring, "Illustrated Anatomy of the Head and Neck", Elsevier, p. 68, 2012.

2- Usama Mahmood, Albert Cerussi, Reza Dehdari, Quoc Nguyen, Timothy Kelley, Bruce Tromberg, Brian Wong, "Near-infrared Imaging of the Sinuses: Preliminary Evaluation of a New Technology for Diagnosing Maxillary Sinusitis", Journal of Biomedical Optics, May/June 2010.

3- U. Mahmood, R. Dehdari, A. E. Cerussi, Q. Nguyen, T. Kelley, B. J.Tromberg, and B. J. Wong, "Near-infrared transillumination of the maxillary sinuses: overview of methods and preliminary clinical results," Proc. SPIE 5686, 333–339, 2005.

4- Sameh M. Ragab, Valerie J. Lund, Glenis Scadding, "Evaluation of the Medical and Surgical Treatment of Chronic Rhinosinusitis: A Prospective, Randomised, Controlled Trial", Article first published online: 3 JAN 2009.

5- M. S. Benninger, B. J. Ferguson, J. A. Hadley, D. Hamilos, M. Jacobs, D. Kennedy, D. Lanza, B. Marple, J. Osguthorpe, and J. Stankiewicz, "Adult Chronic Rhinosinusitis: Definitions, Diagnosis, Epidemiology, and Pathophysiology", Otolaryngol.-Head Neck Surg. 129, S1–32, 2003.

6- Stewart MG1, Sicard MW, Piccirillo JF, Diaz-Marchan PJ, "Severity Staging in Chronic Sinusitis: Are CT scan Findings Related to Patient Symptoms?", American Journal of Rhinology, May-Jun;13(3):161-7, 1999.

7- Aygun N, Zinreich SJ, “Radiology of the Nasal Cavity and Paranasal Sinuses”, In: Cummings CW, Flint PW, Haughey BH, et al, eds. Otolaryngology: Head & Neck Surgery. 5th ed. Philadelphia, Pa: Mosby Elsevier, 2010.

8- Shaw AS, Dixon AK, “Multidetector Computed Tomography”, In: Adam A, Dixon AK, eds. Grainger & Allison's Diagnostic Radiology: A Textbook of Medical Imaging. 5th ed. New York, NY: Churchill Livingstone, 2008.

9- Anslow P. “Ear, Nose and Throat Radiology”, In: Adam A, Dixon AK, Grainger RG, et al., eds. Grainger & Allison’s Diagnostic Radiology: A Textbook of Medical Imaging. 5th ed. Philadelphia, Pa: Elsevier Churchill Livingstone, 2008.

10- Thomas F. Burke, Andrew I. GuertEer, James H. Tinzmons, “Comparison of Sinus X-rays with Computed Tomography Scans in Acute Sinusitis”, Academic Emergency Medicine, May-Jun; 1(3):235-9, 1994.

11- Wilkinson ID, Paley MNJ., “Magnetic Resonance Imaging: Basic Principles”, In: Grainger RC, Allison D, Adam, Dixon AK, eds. Diagnostic Radiology: A Textbook of Medical Imaging. 5th ed. New York, NY: Churchill Livingstone; 2008.

12- Alper Bozkurt, Arye Rosen, Harel Rosen, Banu Onaral, "A Portable Near Infrared Spectroscopy System for Bedside Monitoring of Newborn Brain.". BioMedical Engineering OnLine 4(1): 29. doi:10.1186/1475-925X-4-29. PMC 1112605.PMID 15862131, 2005.

13- Jerrold T. Bushberg, J. Anthony Seibert, Edwin M. Leidholdt, John M. Boone, “The Essential Physics of Medical Imaging”, 2nd ed., Lippincott Williams & Wilkins, 2002.

14- F. W. Otten and J. J. Grote, “The Diagnostic Value of Transillumination for Maxillary Sinusitis in Children,” Int. J. Pediatr. Otorhinolaryngol. 18, 9–11, 1989.

15- Charlie Goldberg, “A Practical Guide to Clinical Medicine”, University of California, San Diego, last updated in 2008.

16- CVIPtools (2010),“Computer Vision and Image processing Tools”. http://cviptools.ece.siue.edu

17- CVIP-FEPC (2010), “CVIP- Feature Extraction and Pattern Classification”. http://cviptools.ece.siue.edu

18- Scott E Umbaugh, “Digital Image Processing and Analysis: Human and Computer Vision Applications with CVIPtools, Second Edition”. The CRC Press, Boca Raton, FL, 2010.